University of Zurich[UZH]

Zurich Open Repository and Archive
University of Zurich
University Library
Strickhofstrasse 39
CH-8057 Zurich
www.zora.uzh.ch

Year: 2012

Identification and functional characterization of pVHL-dependent cell surface proteins in renal cell carcinoma

Boysen, Gunther ; Bausch-Fluck, Damaris ; Thoma, Claudio R ; Nowicka, Anna M ; Stiehl, Daniel P ; Cima, Igor ; Luu, Van-Duc ; von Teichman, Adriana ; Hermanns, Thomas ; Sulser, Tullio ; Ingold-Heppner, Barbara ; Fankhauser, Niklaus ; Wenger, Roland H ; Krek, Wilhelm ; Schraml, Peter ; Wollscheid, Bernd ; Moch, Holger

Abstract: The identification of cell surface accessible biomarkers enabling diagnosis, disease monitoring, and treatment of renal cell carcinoma (RCC) is as challenging as the biology and progression of RCC is unpredictable. A hallmark of most RCC is the loss-of-function of the von Hippel-Lindau (pVHL) protein by mutation of its gene (VHL). Using the cell surface capturing (CSC) technology, we screened and identified cell surface N-glycoproteins in pVHL-negative and positive 786-O cells. One hundred six cell surface N-glycoproteins were identified. Stable isotope labeling with amino acids in cell culture-based quantification of the CSC screen revealed 23 N-glycoproteins whose abundance seemed to change in a pVHL-dependent manner. Targeted validation experiments using transcriptional profiling of primary RCC samples revealed that nine glycoproteins, including CD10 and AXL, could be directly linked to pVHL-mediated transcriptional regulation. Subsequent human tumor tissue analysis of these cell surface candidate markers showed a correlation between epithelial AXL expression and aggressive tumor phenotype, indicating that pVHL-dependent regulation of glycoproteins may influence the biologic behavior of RCC. Functional characterization of the metalloprotease CD10 in cell invasion assays demonstrated a diminished penetrating behavior of pVHL-negative 786-O cells on treatment with the CD10-specific inhibitor thiorphan. Our proteomic surfaceome screening approach in combination with transcriptional profiling and functional validation suggests pVHL-dependent cell surface glycoproteins as potential diagnostic markers for therapeutic targeting and RCC patient monitoring.

DOI: https://doi.org/10.1596/neo.12130

Posted at the Zurich Open Repository and Archive, University of Zurich
ZORA URL: https://doi.org/10.5167/uzh-63574
Journal Article
Published Version

The following work is licensed under a Creative Commons: Attribution-NonCommercial-NoDerivs 3.0 Unported (CC BY-NC-ND 3.0) License.

Originally published at:
Boysen, Gunther; Bausch-Fluck, Damaris; Thoma, Claudio R; Nowicka, Anna M; Stiehl, Daniel P; Cima, Igor; Luu, Van-Duc; von Teichman, Adriana; Hermanns, Thomas; Sulser, Tullio; Ingold-Heppner,

Barbara; Fankhauser, Niklaus; Wenger, Roland H; Krek, Wilhelm; Schraml, Peter; Wollscheid, Bernd; Moch, Holger (2012). Identification and functional characterization of pVHL-dependent cell surface proteins in renal cell carcinoma. Neoplasia, 14(6):535-546.
DOI: https://doi.org/10.1596/neo.12130

NEOPLASIA
www.neoplasia.com

Volume 14 Number 6 June 2012 pp. 535–546 535

Identification and Functional Characterization of pVHL-Dependent Cell Surface Proteins in Renal Cell Carcinoma[1,2]

Gunther Boysen*[,3], Damaris Bausch-Fluck[†], Claudio R. Thoma[‡], Anna M. Nowicka*, Daniel P. Stiehl[§], Igor Cima[‡], Van-Duc Luu*, Adriana von Teichman*, Thomas Hermanns[¶], Tullio Sulser[¶], Barbara Ingold-Heppner*[,4], Niklaus Fankhauser[‡], Roland H. Wenger[§], Wilhelm Krek[‡], Peter Schraml*, Bernd Wollscheid[†] and Holger Moch*

*Institute of Surgical Pathology, University Hospital Zurich, Zurich, Switzerland; [†]Institute of Molecular Systems Biology, ETH Zurich, Zurich, Switzerland; [‡]Institute of Cell Biology, ETH Zurich, Zurich, Switzerland; [§]Institute of Physiology, University of Zurich, Zurich, Switzerland; [¶]Clinic for Urology, University Hospital Zurich, Zurich, Switzerland

Abstract

The identification of cell surface accessible biomarkers enabling diagnosis, disease monitoring, and treatment of renal cell carcinoma (RCC) is as challenging as the biology and progression of RCC is unpredictable. A hallmark of most RCC is the loss-of-function of the von Hippel–Lindau (pVHL) protein by mutation of its gene (*VHL*). Using the cell surface capturing (CSC) technology, we screened and identified cell surface N-glycoproteins in pVHL-negative and positive 786-O cells. One hundred six cell surface N-glycoproteins were identified. Stable isotope labeling with amino acids in cell culture–based quantification of the CSC screen revealed 23 N-glycoproteins whose abundance seemed to change in a pVHL-dependent manner. Targeted validation experiments using transcriptional profiling of primary RCC samples revealed that nine glycoproteins, including CD10 and AXL, could be directly linked to pVHL-mediated transcriptional regulation. Subsequent human tumor tissue analysis of these cell surface candidate markers showed a correlation between epithelial AXL expression and aggressive tumor phenotype, indicating that pVHL-dependent regulation of glycoproteins may influence the biologic behavior of RCC. Functional characterization of the metalloprotease CD10 in cell invasion assays demonstrated a diminished penetrating behavior of pVHL-negative 786-O cells on treatment with the CD10-specific inhibitor thiorphan. Our proteomic surfaceome screening approach in combination with transcriptional profiling and functional validation suggests pVHL-dependent cell surface glycoproteins as potential diagnostic markers for therapeutic targeting and RCC patient monitoring.

Neoplasia (2012) 14, 535–546

Abbreviations: ASAP ratio, automated statistical analysis on protein ratio; ccRCC, clear cell renal cell carcinoma; ChIP, chromatin immunoprecipitation; CSC, cell surface capturing; DMOG, dimethyloxalyl glycine; HIF, hypoxia-inducible factor; HRE, hypoxia response element; LC-MS/MS, liquid chromatography tandem mass spectrometry; LDA, low-density array; MS, mass spectrometry; pRCC, papillary renal cell carcinoma; pVHL, von Hippel–Lindau protein; RCC, renal cell carcinoma; SILAC, stable isotope labeling with amino acids in cell culture; TMA, tissue microarray; VHL, von Hippel–Lindau

Address all correspondence to: Prof. Dr.med. Holger Moch, MD, Institute of Surgical Pathology, University Hospital Zurich, Schmelzbergstrasse 12, 8091 Zurich, Switzerland. E-mail: holger.moch@usz.ch; or Bernd Wollscheid, PhD, Institute of Molecular Systems Biology (IMSB), ETH Hönggerberg, HPT D77, Wolfgang Pauli-Str. 16, CH-8093 Zürich, Switzerland. E-mail: wbernd@ethz.ch

[1]This study was supported by UBS AG to P.S. (made possible by an anonymous donor), the Swiss National Cancer Foundation to H.M. (3238BO-103145), the Zurich Cancer League to H.M. and B.W., and the National Center of Competence in Research Neural Plasticity and Repair to B.W.

[2]This article refers to supplementary materials, which is designated by Tables W1 to W9 and Figures W1 and W2 and are available online at www.neoplasia.com.

[3]Present address: Department of Pathology, Weill Cornell Medical College, New York, NY.
[4]Present address: Institute of Pathology, Campus Mitte, Charitè-Universitätsmedizin, Berlin, Germany.

Received 6 January 2012; Revised 27 April 2012; Accepted 30 April 2012

Copyright © 2012 Neoplasia Press, Inc. All rights reserved 1522-8002/12/$25.00
DOI 10.1596/neo.12130

Introduction

The prognosis of advanced renal cell carcinoma (RCC) is poor. Most RCC cases are insusceptible to chemotherapies or radiotherapies, which seems to be partly caused by a hypoxia-mediated resistance to radiotherapy and alkylating agents [1–4]. Since 2006, novel anti-angiogenic targeted therapies have been available for patients with metastatic RCC. These therapies rely on a targeted blockade of angiogenic signaling caused by an aberrant overexpression of proangiogenic cell surface proteins, for example, vascular endothelial growth factor and platelet-derived growth factor as well as their corresponding receptors [5–8]. Despite these novel drugs, identification of additional cellular treatment targets, screening markers for early stages, recurrent tumors after nephrectomy, and predictive markers for treatment response is of utmost importance to further improve prognosis of RCC patients.

The discovery of cell surface glycoprotein biomarkers for RCC would be clinically useful because these glycoproteins are exposed to the cellular microenvironment and are, therefore, easily accessible by affinity-based probes such as drugs and antibodies for disease monitoring. Furthermore, cell surface glycoproteins can be shed into the bloodstream and could provide potential targets for recently developed remote-sensing serum-screening strategies [9]. However, the identification of the cellular surfaceome is challenging owing to its lower abundance compared with intracellular subproteomes, its hydrophobicity due to transmembrane domains, and the high degree of posttranslational modifications on these proteins. One solution to overcome this abundance problem is to focus on the cotranslational modification of cell surface proteins with glycostructures. The recently developed mass spectrometry (MS)–based cell surface capturing (CSC) technology is through the glycosylation of cell surface proteins for specific enrichment of this subproteome and subsequent identification [10]. Glycoproteins are also of particular clinical interest given that approximately 80% of all current protein drug targets are glycoproteins [11].

Strategies for the identification of RCC glycoprotein biomarkers can be combined with available knowledge about cancer-causing mutations. The von Hippel–Lindau (*VHL*) gene is the most commonly inactivated gene in the most frequent subtype clear cell RCC (ccRCC). More than 70% of ccRCCs are characterized by somatic mutations or hypermethylation of *VHL* [12–16], whereas in the rare papillary and chromophobe RCC subtypes, *VHL* is hardly affected. *VHL* encodes two proteins of 30 and 19 kDa, the latter being a result of an alternative, in-frame translation initiation codon [17]. Both proteins seem to differ in part in their subcellular localization, which may imply potential functional differences [18,19]. The most described function of pVHL is its role as a substrate recognition component of an E3 ubiquitin protein ligase complex known to target the α-subunits of the hypoxia-inducible factor (HIF) for ubiquitin-mediated proteolysis in a prolyl-4-hydroxylation–dependent manner under normoxic conditions [20–23]. HIF is a sequence-specific heterodimeric transcription factor composed of an α subunit (HIF-1α, HIF-2α, or HIF-3α) and an invariable β subunit. It promotes adaption and survival under low oxygen by up-regulation of genes that are involved in neovascularization, pH regulation, glucose uptake and glycolysis, apoptosis, and cell cycle [24]. In ccRCC, the HIF transcriptional program is uncoupled from changes in oxygen availability and co-opted by the cancer cell to promote tumor growth. Interestingly, vascular endothelial growth factor and platelet-derived growth factor, the two major angiogenic factors successfully targeted by the current above-mentioned therapies, are HIF target genes.

Here we used the CSC technology to screen and identify N-glycosylated cell surface proteins in pVHL-negative and -positive cell lines. The pVHL-dependent glycoproteins detected within the initial screen were subsequently verified and validated *in vitro* and *in situ* at the transcript and at the protein level by using a combination of low-density arrays (LDAs) and tissue microarrays (TMAs), respectively. Our pVHL-guided proteomic surfaceome screening approach in combination with transcriptomic validation and functional characterization revealed pVHL-regulated glycoproteins as candidates for the clinical use in patients with RCC.

Experimental Procedures

Cell Culture and Metabolic Labeling

The ccRCC-derived cell line 786-O, the human embryonic kidney cell line HEK-293, and the human fibrosarcoma cell line HT-1080 were supplied by American Type Culture Collection (Manassas, VA). Stable transfectants of 786-O reexpressing $pVHL_{30}$ were generated as mentioned before [19]. RCC4 cells and their corresponding transfectants reexpressing wild-type $pVHL_{30}$ were created as previously described [19,25]. Human renal proximal tubular epithelial cell line HK-2 was provided by R. Wüthrich (Clinic for Nephrology, Department of Internal Medicine, University Hospital Zurich, Zurich, Switzerland). RCC4, 786-O, HEK-293, and HK-2 cells were cultured as reported previously [26]. Hypoxic experiments were performed for 16 hours at 1% oxygen using a hypoxic workstation ($Invivo_2$ 400; Ruskinn Technology, Leeds, United Kingdom). Dimethyloxalyl glycine (DMOG) (Cayman Chemical, Ann Arbor, MI) treatment was performed for 24 hours at 1 mM. Stable isotope labeling with amino acids in cell culture (SILAC) was used for the *in vivo* incorporation of isotopically labeled amino acids into all cellular proteins. For SILAC labeling, 786-O and their stable transfectants reexpressing $pVHL_{30}$ were grown in L-lysine and L-arginine–deficient Dulbecco modified Eagle medium (Sigma) containing 10% vol/vol dialyzed fetal calf serum (FCS), 2 mM glutamine, and either normal or heavy lysine/arginine. Cells were grown for five to six generations. Then, 5×10^7 786-O and 786-$OpVHL_{30}$ were used for CSC.

CSC-Based Proteomic Surfaceome Screen

Cells were labeled in 10 ml of labeling buffer containing 5 mM biocytin hydrazide for 60 minutes. On labeling, the cells were harvested by scraping. Oxidation of cell surface glycoproteins subsequent cell surface labeling, cell lysis, membrane preparation, and final processing, and isolation of N-glycopeptides was performed as described in Wollscheid et al. [10].

Mass Spectrometry

Peptide samples were analyzed on a hybrid LTQ-FT-ICR instrument (Thermo Electron, Bremen, Germany) interfaced with a nanoelectrospray ion source. Before the LTQ-FT-ICR analysis, peptides were separated on a RP-HPLC column (75 μm × 15 cm) packed in-house with C18 resin (Magic C18 AQ 3 μm; Michrom BioResources, Auburn, CA) using a linear gradient from 96% solvent A (0.15% formic acid) and 4% solvent B (98% acetonitrile, 2% water, 0.15% formic acid) to 25% solvent B for 60 minutes at a flow rate of 300 nl/min performed by a Tempo Nano 1D+ HPLC system (Applied Biosystems/MDS Sciex, Foster City, CA).

Each MS1 scan was followed by CID scans of the five most abundant precursor ions with dynamic exclusion for 30 seconds. Only MS1 signals exceeding 150 counts were allowed to trigger MS2 scans with wideband activation disabled. Total cycle time was approximately 1 to 1.5 seconds. For MS1, 3×10^6 ions were accumulated in the ICR cell for a maximum time of 500 milliseconds and scanned at a resolution of 100,000 full width at half maximum (at 400 *m/z*). MS2 spectra were acquired in the linear trap using the normal scan mode, a target setting of 10^4 ions and accumulation time of 100 milliseconds. In the LTQ-FT analysis, singly charged ions and ions with unassigned charge state were excluded from triggering MS2 events. The normalized collision energy was set to 32%, and one microscan was acquired for each spectrum.

Data Analysis

The raw data acquired by the LTQ-FT instrument (software, Xcalibur 2.0; Thermo Scientific, Waltham, MA) was converted to mzXML using ReAdW (3.5.1) applying default parameters. MS/MS scans were searched against the human International Protein Index (IPI, version 3.15, 58099 protein entries) database using SEQUEST version 27 with the following parameters. For LTQ-FT data, precursor mass tolerance was set to 0.1 Da, a minimum of one tryptic termini was allowed, and variable modifications were allowed on asparagines (0.9840), on lysines (8.014199), and on arginines (10.008269), with a maximum of four modifications per peptide. No static modifications were defined. Data were further processed by the Trans-Proteomic Pipeline TPP v2.9 including PeptideProphet and ProteinProphet to estimate the false discovery rate. A protein probability cutoff of 0.8 was used, which corresponds to a false discovery rate of approximately 1%.

Quantification

For obtaining quantitative ratios between the differentially SILAC-labeled samples, we applied automated statistical analysis on protein (ASAP) ratio v3.0 [27]. The algorithm was run with a fixed scan range for the light and the heavy ions and with no background subtraction for the peak integration. ASAP ratio is an integrated part of the TPP and it normalizes the ratio distribution and computes a protein ratio. The results were curated manually.

RNA Isolation and LDA Applications

RNA from frozen tissue was isolated using the RNAeasy Mini Kit (Qiagen, Hilden, Germany). The quality and quantity of the isolated RNA were analyzed by means of nanodrop and Agilent Bioanalyzer 2100. Reverse transcription of isolated RNA was performed by the High-Capacity cDNA Reverse Transcription Kit (Applied Biosystems) according to the manufacturer's instructions. Pilot experiments using RNA derived from tumor cell lines and tissue were performed with selected TaqMan gene expression assays to verify the reverse transcription step linearity and to determine the amount of cDNA, which can be loaded in polymerase chain reaction (PCR) without inhibition. Applied Biosystems TaqMan LDAs were configured using the online software tool TaqMan Custom Array (https://products.appliedbiosystems.com). Only assays whose probes span an exon junction were chosen to avoid detection of genomic DNA. Preparation and loading of the sample-specific PCR mix into the fill reservoirs of the TaqMan Microfluid Cards were accomplished according to the manufacturer's instructions. Relative levels of gene expression were determined from the fluorescence data generated during PCR using the Applied Biosystems 7900HT Fast Real-Time PCR System followed by computational analysis by means of SDS and RQ manager software with HPRT1 and 18S rRNA as internal control.

Quantitative Reverse Transcription–PCR

Total RNA from pools of clones of 786-O and 786-OpVHL_{30} cells, lentivirally infected with shHIF-2α (target constructs 1 and 4) as well as uninfected control cells, was prepared using the RNAeasy Mini Kit (Qiagen) according to the manufacturer's protocol. Reverse transcription was performed by High-Capacity cDNA Reverse Transcription Kit (Applied Biosystems). cDNA reverse transcribed from 50 ng of total RNA was used for quantitative reverse transcription (RT)–PCRs containing 10 μl of TaqMan 2× PCR MasterMix (Applied Biosystems) and 1 μl of TaqMan Gene Assay (Applied Biosystems) for CD10 (Hs00153519_m1) or 200 nM primers and 100 nM of the universal probe library probe 55 (Roche, Mannheim, Germany) for HIF-2α in a volume of 20 μl. Detection was carried out with a Fast Real-Time PCR System (7900HT; Applied Biosystems). Data analysis was performed using the SDS and RQ manager software (Applied Biosystems). Peptidyl-prolyl *cis-trans* isomerase A (PPIA) served as an internal control (Hs99999904_m1).

Tissue Specimen and TMA Construction

We used TMAs comprising 264 ccRCC collected from the University Hospital of Zurich (Zurich, Switzerland) to validate the *in vitro* data. All tissue samples were histologic reviewed by one pathologist (H.M.) and selected on the basis of hematoxylin and eosin–stained tissue sections [28]. A more comprehensive TMA study was performed to confirm the HIF dependence of CD10 in ccRCC. We used three TMAs comprising 831 ccRCC collected at the University Hospital of Zurich (Zurich, Switzerland), the Kantonsspital St. Gallen (St. Gallen, Switzerland), and the University Hospital of Basel (Basel, Switzerland). The composition of the TMAs and clinicopathologic data were previously described [29]. This study was approved by the local ethics commission (reference number StV 38-2005).

Immunohistochemistry

TMA sections (2.5 μm) were transferred to glass slides followed by immunohistochemical analysis according to Ventana automat protocols (Ventana Medical System, Tucson, AZ). Antibodies were applied for detection of AXL (1:200, AF154; R&D Systems, Planegg-Martinsried, Germany), CAIX M75 (1:200; kindly provided by J. Zavada, Institute of Molecular Genetics, Prague, Czech Republic), CD10 (1:30, NCL-CD10-270; Novocastra Laboratories, Newcastle, United Kingdom), CD13 (1:200, NCL-CD13-304; Novocastra Laboratories Ltd), CD31, CD34, CD99 (1:25, NCL-CD99; Novocastra Laboratories Ltd), CCND1 (prediluted, Ventana, P2D11F11 [29]), E-CADH (1:10, ECH-6; Cell Marque, Rocklin, CA), and SLC2A1 (GLUT-1) (1:1000, AB1341; Chemicon, Temecula, CA). Analysis was performed with a Leitz Aristoplan microscope (Leica Microsystems, Wetzlar, Germany). Pictures of ccRCC specimens were obtained with a digital camera (KY-070; JVC, Friedberg, Germany). The intensity of the staining for AXL, CAIX, CD10, CD13, E-CADH, and GLUT-1 was classified as follows: 0 no, +1 weak, or +2 strong membranous staining. Endothelial AXL was analyzed to measure the microvessel density of the tumors as follows: 1 = low (0-10), 2 = median (>10-50 cells), and 3 = high

(>50 cells). Immunostained TMAs were scanned using the NanoZoomer Digital Slide Scanner (Hamamatsu Photonics K.K., Shizuoka, Japan).

Immunoblot Analysis

Cell and tissue lysates were prepared using RIPA buffer (Sigma, Steinheim, Germany) containing complete protease inhibitor cocktail (Roche). Homogenization was performed with a Tissue lyser (Qiagen) for 4 minutes at 20 Hz. Lysates were centrifuged for 10 minutes (2500*g*, 4°C). Protein concentration of the supernatant was determined by the BCA Assay (Pierce, Rockford, IL) with bovine serum albumin (BSA) as a standard. The following primary antibodies were used for the functional characterization of CD10: mouse monoclonal anti–CA9 M75 (kindly provided by J. Zavada, Institute of Molecular Genetics; 1:1000), mouse monoclonal anti-CD10 (NCL-CD10-270; Novocastra Laboratories; 1:100), rabbit polyclonal anti–Glut-1 (AB1341; Chemicon; 1:4000), rabbit polyclonal HIF-2α (NB100-122; Novus Biologicals, Littleton, CO; 1:1000), mouse monoclonal anti–β-actin (Chemicon; 1:10,000), and rabbit polyclonal α-pVHL$_{CT}$ [19] (1:500). After washing with Tris-buffered saline Tween 20, the membranes were incubated at room temperature with HRP-conjugated secondary antibody rabbit anti-mouse (Abcam, Cambridge, United Kingdom; 1:3000) or goat anti-rabbit (MAB1501; Chemicon; 1:3000). The protein-antibody complexes were detected by ECL (Amersham, Piscataway, NJ). Biotinylation of proteins was determined by incubating membranes with streptavidin-HRP (1:5,000). The protein-antibody/biotin-streptavidin complexes were detected by ECL (Amersham).

ELISA

CD10 concentration in human serum samples of 21 RCC and 6 healthy controls was measured by ELISA (R&D Systems). This study was approved by the local ethics commission (EK-1017). The patients' sera were collected according to the standardized protocol of the Department of Urology, University Hospital Zurich. Capture antibody was coated overnight at 4°C in 50 mM Tris-HCl, pH 9.4. Plates were subsequently blocked using 1% BSA in phosphate-buffered saline. Samples were diluted 1:5 in diluent buffer, comprising of 1:3 LowCross Buffer (Candor Bioscience, Eggenwatt, Weissensberg), 0.1% goat serum, and 1% BSA in phosphate-buffered saline for 2 hours at room temperature. The biotinylated detection antibody was diluted in diluent buffer and incubated for 2 hours at room temperature followed by 20 minutes of incubation with streptavidin-HRP and substrate detection. The serum diluent was shown in separate experiments to efficiently inhibit false-positive and false-negative signals. Interassay and intra-assay variations were less than 3% and less than 20%, respectively.

Short Hairpin RNA Constructs and Lentiviral Infections

Expression vectors encoding short hairpin RNA (shRNA) sequences targeting human HIF-2α were purchased from Sigma (shHIF-2α#1, clone ID NM_001430.x-517s1c1; and shHIF-2α#4, clone ID NM_001430.x-1694s1c1, respectively). Viral particles were produced using the ViraPower lentiviral expression system according to the manufacturer's instructions (Invitrogen). Briefly, 786-O cells were infected with lentiviral particles of either shHIF-2α#1 or shHIF-2α#4 constructs, and pools of clones were derived by puromycin selection (4 μg/ml). Pools of clones were analyzed for effective HIF-2α knockdown by quantitative RT-PCR and anti–HIF-2α immunoblot analysis.

Reporter Gene Assay

Four different *CD10* promoter fragments were obtained by PCR amplification of human genomic DNA. The oligonucleotide primers used in this study are summarized in Table W9. PCR products were sequenced using the AbiPrism 3100 Genetic analyzer (Applied Biosystems). The reporter constructs were generated by insertion of individual *CD10 Kpn*I-*Nhe*I fragments from the human *CD10* promoter into the *Kpn*I-*Nhe*I sites of a promoterless pGL4.10 firefly luciferase reporter gene plasmid (Promega, Madison, WI). Site-directed mutation of HREI in the *CD10* promoter was performed on pGL4.10 containing the whole *CD10* promoter using the QuickChange II Site-Directed Mutagenesis Kit (Stratagene, Cedar Creek, TX). For transcriptional transactivation experiments, HEK-293 and HK-2 cells were transfected with 1 μg of reporter plasmids along with 100 ng of pGL4.74 renilla luciferase reporter plasmid (Promega) in 24-well plates using FuGene 6 reagent (Roche). pGl3P2P(607 bp) vectors are 5′-truncated versions of the previously published pGl3b(1454/3172)P2P plasmids containing the wild-type or mutated hypoxia response element (HRE) of the human PHD2 promoter [30]. These vectors served as positive or negative controls for HIFα activity. The empty pGL4.10 vector served as MOCK control. Luciferase activity was measured after cell lysis using the dual-luciferase reporter assay system (Promega). Luciferase activities were determined by dividing the relative luciferase units from hypoxic/DMOG–treated and normoxic/untreated cells. Renilla luciferase control reporters were used for normalization of transfection efficiency.

Chromatin Immunoprecipitation

Chromatin immunoprecipitation (ChIP) was performed according the protocol (version 10.0) of mammalian ChiP-on-chip (Agilent Technologies). Briefly, 5×10^7 to 1×10^8 cells grown in normoxia or hypoxia were fixed in 1% formaldehyde, washed, harvested, and lysed. The cell lysates were sonicated to fragment cellular DNA into fragments of 100 to 600 bp in size and incubated with an anti–HIF-1α (mouse monoclonal, NB100-105; Novus Biologicals) antibody/magnetic bead (Dynabeads Potein G; Invitrogen) mixture overnight at 4°C. After washing to deplete unbound DNA, elution of bounded DNA/antibody complexes from the beads was performed in elution buffer at 65°C. Beads were separated from the eluent by centrifugation (16,000*g*, 1 minute). Cross-linking of DNA and antibody was reversed by incubating the supernatant at 65°C overnight. Finally, cellular protein and RNA were digested by means of proteinase K and RNase A. DNA was extracted by means of phenol-chloroform-isoamyl alcohol in Phase Lock Gel tubes (Eppendorf, NY). DNA concentrations were measured using a nanodrop. SYBR Green Real-time PCR was performed with 10 ng of isolated DNA in a 20-μl reaction using a 7900HT PCR cycler (Applied Biosystems) to quantify the differential binding of HIF-1α to the analyzed HREs of *CD10*. The primers used for the ChIP experiments are listed in Table W9.

Cell Invasion Assay

Cell invasion was assessed using the QCM 24-well fluorometric cell invasion assay (Millipore, Zug, Switzerland) according to the manufacturer's protocol. Cells were starved in serum-free medium for 24 hours. Afterward, 0.5×10^6 cells/ml were seeded into extracellular matrix–coated inserts and cultured for 72 hours. FCS was used as a chemoattractant in the bottom chamber. The CD10

inhibitor thiorphan (Merck, Darmstadt, Germany) was added to the bottom chamber using the following final concentrations: 1 and 10 μM, respectively.

Statistical and Computational Analyses

Contingency table analysis, Pearson χ^2 tests, Kaplan-Meier curves, and log-rank tests for evaluating correlations between AXL, CD10, CD13, GLUT-1, and E-cadherin expression and clinical parameters were calculated using StatView (SAS, Institute, Cary, NC). One-tailed unpaired *t* test with Welsch correction to compare CD10 serum levels in tumor patients with healthy controls was performed using GraphPad Prism 4 (GraphPad Software, San Diego, CA). Automatic classification of the LDA expression data was performed using pocus [31] and R [32] package for assessing the uncertainty in hierarchical cluster analysis by resampling. Average linkage clustering was performed with correlation as a distance measure using 1000 bootstrap replications. The random forest algorithm, implemented as R package, was used for unsupervised classification. It was set to assess the importance of predictors.

Results

Identification of pVHL-Dependent Cell Surface N-glycoproteins in ccRCC

The CSC technology was used as an initial screen to identify potentially pVHL-dependent cell surface N-glycoproteins. In brief, cell surface–exposed glycans were oxidized and tagged with biocytin hydrazide. Then, the cells were lysed, proteins were digested, and the tagged peptides were captured with streptavidin. After thorough washing, N-glycosylated peptides were released with peptide N-glycosidase F, cleaned up with C18 tips, and subjected to liquid chromatography tandem mass spectrometry (LC-MS/MS) analysis. In a first step, we combined SILAC- and CSC-based labeling and isolation of N-glycosylated cell surface N-glycoproteins from ccRCC-derived 786-O cells and stable transfectants reexpressing the long form of wild-type pVHL (referred to as 786-OpVHL$_{30}$). Subsequent shotgun proteomics analysis of enriched N-glycosylated plasma membrane proteins from 786-O and 786-OpVHL$_{30}$ cells resulted in the identification of 110 proteins (peptide prophet score ≥ 0.8) (Tables W1–W4 and Figure W1). The 106 proteins, which contained a peptide with at least one consensus N-glycosylation motif (NXS/T), were subjected to further analysis (Table W5). In a first *in silico* functional classification procedure using the Panther (www.pantherdb.org) and IPA (Ingenuity Systems) classification tools, we uncovered significant enrichments of proteins whose functions have been associated with cell adhesion and cell communication (Figure 1*A*). A second analysis focused on the involvement of the proteins in specific well-described canonical pathways. The identified proteins are mostly involved in signaling cascades mediated by integrins, cadherins, and Wnt (data not shown).

Quantification of the pVHL-Dependent Cell Surface N-glycoproteins

SILAC-based labeling of the screened glycoproteins in 786-O and 786-OpVHL$_{30}$ allowed for the initial relative quantification of 63 cell surface proteins (Table W5). Twenty-three proteins (20.5%) met the criteria of differential expression between pVHL-negative and pVHL$_{30}$-positive 786-O (ASAP ratio $0.33 > x > 3$). Differential expression of the HIF target GLUT-1 served as control for the activity of the HIF pathway and demonstrated the reliability of the measurements

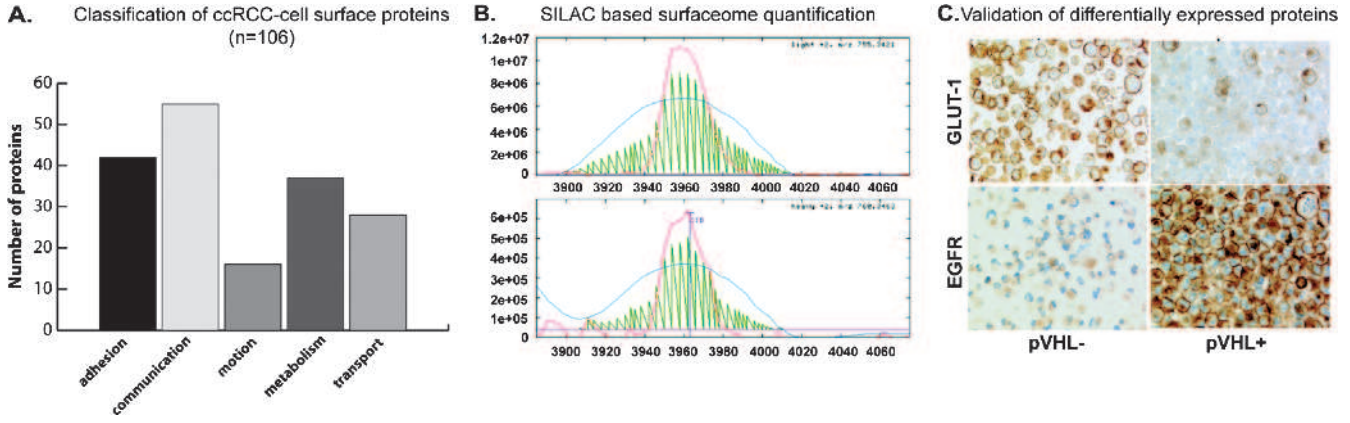

Figure 1. *In silico* characterization of the identified cell surface proteins. (A) Most prominent molecular pathways at which the identified cell surface proteins participate. The functional classification of all identified proteins ($n = 106$) has been performed by using the PANTHER and KEGG databases. (B) Relative protein expression profiling in ccRCC-derived cells using metabolic labeling of proteins by SILAC and LC-MS/MS–based peptide identification. pVHL expressing or pVHL-negative 786-O cells were grown in medium containing heavy- or light-labeled L-Arg/L-Lys isotopes, respectively. Ratios of the peak intensity were computationally calculated by the ASAP ratio algorithm for every peptide. Shown in the figure is the reconstructed MS1 signal of a pair of light/heavy GLUT-1 peptides detected in pVHL-positive and -negative cells in the ASAP ratio view. The ratios of the same peptide in different charge states are averaged and weighted by the corresponding spectrum intensity to obtain the peptide light-heavy ratio and its error. Up-regulation of GLUT-1 in pVHL (light-labeled) 786-O cells compared with their pVHL-reexpressing transfectants (heavy-labeled) functioned as internal control for the activity of the HIF pathway. (C) Immunohistochemical validation of the expression of GLUT-1 and EGFR on formalin-fixed and paraffin-embedded 786-O cells. pVHL− indicates 786-O cells lacking the pVHL protein. pVHL+ indicates 786-O cells reexpressing pVHL. The top row represents cells stained for GLUT-1. The bottom row represents cells stained for EGFR. Figure 3*C* was modified from Boysen et al. (*Pathologe*, 2009;30 Suppl 2:188–192). With permission from Springer Science and Business Media.

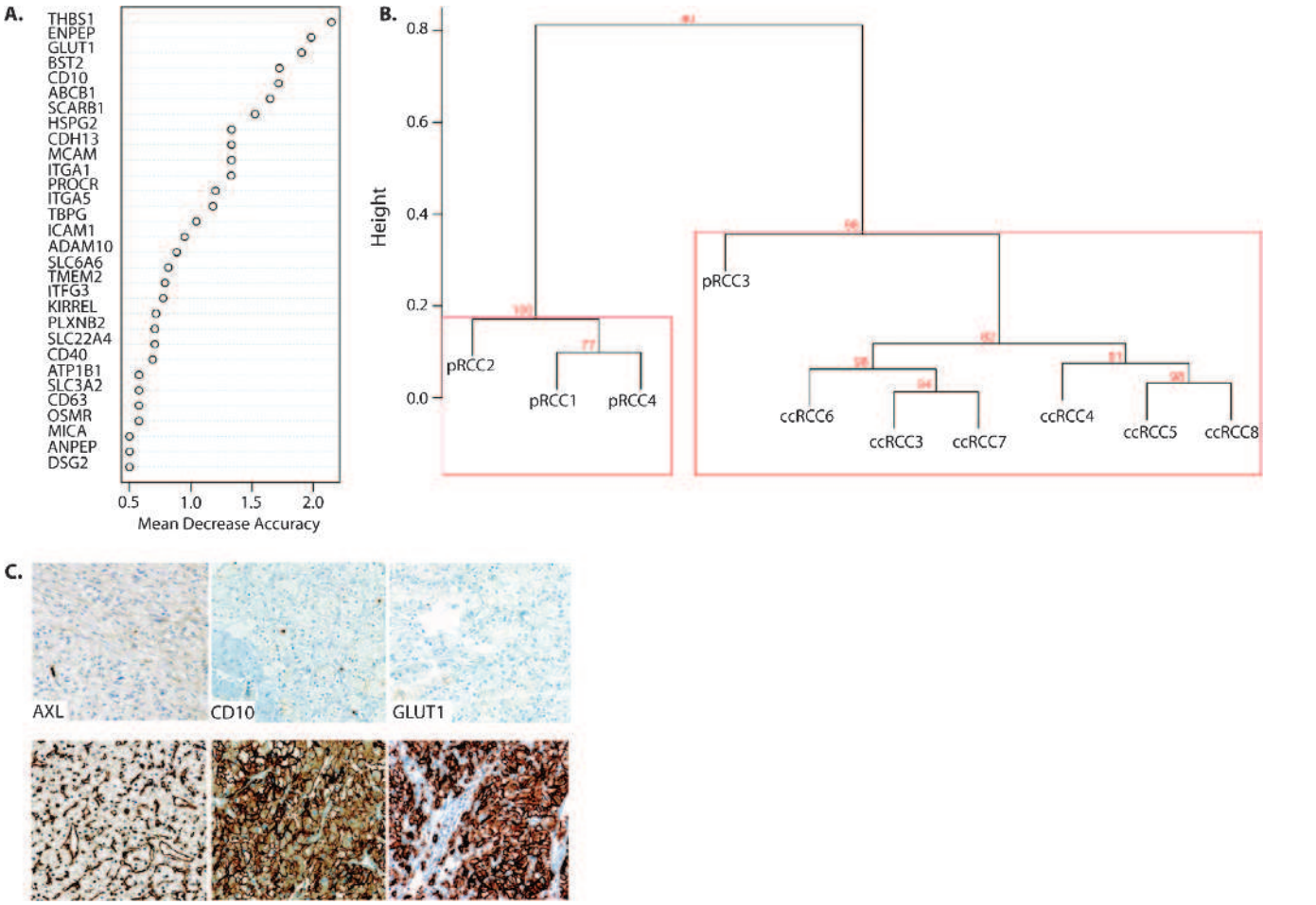

Figure 2. Supervised hierarchical clustering on genes analyzed by LDA in the two major subtypes of RCC. (A and B) Molecular subtyping based on gene expression data derived from 10 RCC samples analyzed by LDAs correlated mostly with the histologic features of the tumors. Histologic subtypes are named as follows: pRCC—papillary RCC and ccRCC—clear cell RCC. Genes that differentiate most significantly between the histologic subtypes are listed. (C) TMA-based expression analyses of selected candidates from the initial *in vitro* and *in vivo* measurements. Shown are examples of positive and negative tumors for each protein analyzed.

(Figure 1*B*). Immunohistochemical validation on formalin-fixed and paraffin-embedded 786-O and 786-OpVHL$_{30}$ cells confirmed the quantitative MS/MS data (Figure 1*C*).

In silico functional classification of the 23 differentially expressed proteins using the Panther database suggested these proteins to participate in cell proliferation (EGFR signaling), cell cycle regulation (p53 signaling), and cell motility (integrin and cadherin signaling) (data not shown).

LDA-Based Validation of RCC-Associated Cell Surface N-glycoproteins in Cell Lines and Primary Tumors

In a second step we combined discovery-driven proteomic screening data with transcriptomic profiling of the preliminary 106 candidates for validation *in vitro*. The identified cell surface N-glycoproteins were validated *in vitro* by using a customized LDA platform. HPRT1 mRNA and 18S rRNA were used for normalization of gene expression. Real-time RT-PCR–based amplification of cDNA was detected for 82 candidates (73.2%; Table W7). Of 23 pVHL-dependent proteins, 15 (65%) also showed a pVHL-related transcriptional regulation (Table W7).

To validate the pVHL-dependent transcriptionally regulated candidates from the 786-O cells in human tissue samples, we expanded our targeted LDA analysis to RNA samples from ccRCC (n = 6), pRCC (n = 4), and normal kidney tissue samples (n = 5, pooled). Of the 73 detectable genes, 34 (46.6%) were differentially expressed in ccRCC compared with normal kidney (Table W8). Of 73 detectable genes, 25 (34.3%) were differentially expressed in ccRCC compared with pRCC or normal kidney (Table W8). Thus, we identified significant differences between normal and tumor tissues suggesting the existence of a tumor subtype-specific signature. Random forest [33] and bootstrapping algorithms (pvclust) identified the genes that most accurately distinguished between both RCC subtypes (Figure 2*A*). The genes *THBS1*, *ENPEP*, *SLC2A1*, *BST2*, *MME* (*CD10*), *ABCB1*, and *SCARB1* were identified, among others, as important discriminators between both renal carcinoma subtypes. To select proteins for subsequent focused tissue-based analysis, we compared the transcriptomic data obtained from cell lines and tissue samples. This resulted in a final list of nine genes that showed concerted deregulation in cell lines and tissues (Table 1).

Moreover, to further study the difference between ccRCC and pRCC, we performed hierarchical clustering using multiscale bootstrap

Table 1. Final List of Candidate Cell Surface Proteins Specific for ccRCC.

Number	Name	IPI	Entrez	Protein 786-O/786-OpVHL$_{30}$	RNA 786-O/786-OpVHL$_{30}$	RNA ccRCC/pRCC	RNA ccRCC/Normal
1	AXL	00296992	558	0.27	1.75	1.53	2.44
2	BCAM	00002406	4059	1.21	0.23	1.45	0.23
3	CDH2	00290085	1000	0.88	2.04	0.83	4.88
4	CDH6	00024035	1004	1.27	0.37	0.27	3.40
5	F3	00010338	2152	0.22	11.11	0.58	0.10
6	HEG1	00297263	57493	NA	1.82	2.24	0.57
7	MME	00247063	4311	NA	3.7	9.6	0.8
8	SLC22A4	00171334	6583	1.5	2.2	3.0	13.9
9	SLC2A1	00220194	6513	5.5	2.9	8.5	2.2

Genes deregulated on the protein and mRNA level in 786-O cells and differentially expressed in ccRCC compared with pRCC and normal kidney.
NA indicates not analyzed.

resampling (pvclust) of the low-density expression data. This analysis revealed significant tumor subtype–dependent clustering based on differentially expressed cell surface N-glycoproteins (Figure 2*B*).

TMA-Based Expression Analysis of Selected Human RCC-Specific Protein Candidates

We next performed immunohistochemical expression analysis of three of the nine candidates listed in Table 1 for which specific antibodies were commercially available. We analyzed the expression patterns of AXL, CD10, and GLUT-1 using a TMA that contained 264 ccRCC (Figures 2*C* and W2). The associations with pathologic parameters are listed in Table 2.

AXL protein expression was observed in both tumor cells and endothelial cells. Only 23 (10.6%) of ccRCCs presented a strong membranous expression in tumor cells. Epithelial AXL expression correlated strongly with poor differentiation grade (P = .0002) and sarcomatoid differentiation of tumor cells (P < .0001).

A high density of AXL-positive endothelial cells correlated significantly with high nuclear differentiation grade (P < .0001). An inverse correlation was found between a high density of AXL-positive endothelial cells and sarcomatoid differentiation (P < .0001). A high endothelial density determined by AXL correlated with a better patient outcome (P = .0028, log-rank test).

CD10 positivity was mainly observed in nonnecrotic ccRCC (P = .0004) and strong GLUT-1 expression was found primarily in tumors with lower nuclear differentiation grade (P < .0001). There were no associations with patient survival.

CD10 Is a HIF Regulatory Target in ccRCC

As CD10 was identified as a pVHL-regulated protein, we asked whether *CD10* is also regulated by HIF similar to known HIF targets *CAIX* and *GLUT-1*. We first investigated CD10 expression in VHL-negative RCC4 and 786-O cell lines as well as in stable transfectants reexpressing pVHL (RCC4-pVHL$_{30}$, 786-O-pVHL$_{30}$). Immunoblot analysis demonstrated CD10 up-regulation in pVHL-negative cell lines compared with pVHL reexpressing cells (Figure 3*A*). HIF-2α protein levels and the expression of the HIF target gene *GLUT-1* correlated with the expression of CD10 (Figure 3*A*).

CD10 expression increased under hypoxia (1% oxygen) in HK-2 and RCC4-pVHL$_{30}$ cells but remained unchanged at high levels under normoxic and hypoxic conditions in pVHL-negative RCC4 (Figure 3*B*). The increase of CD10 expression correlated with an increase of HIF-1α and HIF-2α in RCC4pVHL30 cells. In HK-2 cells, only an increase in HIF-1α was detectable, suggesting that *CD10* is regulated by both HIF-1α and HIF-2α in a cell type–specific manner (Figure 3*B*). To confirm up-regulation of *CD10* by HIF-2α in ccRCC, shRNA against HIF-2α was expressed in 786-O using two different short hairpin constructs (shHIF-2α#1, shHIF-2α#4). The expression of each construct resulted in a significant reduction of HIF-2α in 786-O on the RNA and the protein levels, which was accompanied by a decrease of CD10 mRNA and protein in VHL-negative 786-O cells (Figure 3, *C* and *D*). This strongly suggests that *CD10* expression is regulated by the pVHL-HIF axis.

Next, a computer-assisted search was performed to investigate a 4-kb genomic DNA fragment of the 5′ region flanking the *CD10* gene (EMBL: X79438) for the presence of the HRE RCGTG (R corresponds to A or G) [34–37]. Four potential HREs were identified in this region. The binding of HIF-1α at the identified HREs was investigated by using the ChIP approach (Figure 4*A*). This analysis could not be performed with HIF-2α because of the lack of antibodies suitable for ChIP analysis. The ChIP experiments were performed in HEK-293 cells cultured in normoxia or hypoxia (1% O_2). Hypoxia induced direct binding of HIF-1α to all four identified HREs in the 5′ region of *CD10*. The strongest accumulation of HIF-1α under hypoxic conditions was found at HREII. No binding of HIF-1α was measured for the negative control gene *KCNJ5*. Initial experiments using IgG isotype control antibodies revealed no increased binding after hypoxic treatment.

We then performed luciferase reporter gene assays to confirm whether HIF binding at the identified HREs in the 5′ region of *CD10* leads to increased luciferase activity. For this purpose, a DNA fragment containing the 5′ region of *CD10* (CD10$_{(-5134/-1005)}$) was inserted upstream of the luciferase cDNA. After transient transfection, HK-2 cells were treated with or without DMOG. DMOG is a prolyl-4-hydroxylase inhibitor resulting in normoxic HIFα stabilization and increased HIF activity. Compared with untreated cells, the luciferase activity of the CD10$_{(-5134/-1005)}$ reporter gene construct was increased 2.3-fold in HK-2 (Figure 4*B*). Specificity of DMOG-induced HIF activity was shown by using a reporter construct harboring wild-type HREs of the HIF target gene *prolyl-4-hydroxylase domain* (*PHD*) *2* promoter (P2P) [30]. A 3.9-fold induction of the P2P wild-type reporter (P2PWT) in HK-2 indicated the activation of HIF after DMOG treatment.

The effect of HIF stabilization on *CD10* activation was also investigated under hypoxic conditions. HK-2 cells transfected with the CD10$_{(-5134/-1005)}$ reporter construct showed a 1.8-fold increase of luciferase activity compared with normoxia. These results confirmed that, in human renal epithelial cells, HIFα stabilization leads to *CD10* promoter activation.

Table 2. TMA-Based Expression Analysis in ccRCC.

Characteristic	AXL Epithelial			AXL Endothelial			CD10			GLUT-1		
	Negative, *n* (%)	Weak, *n* (%)	Strong, *n* (%)	Low, *n* (%)	Moderate, *n* (%)	Strong, *n* (%)	Negative, *n* (%)	Weak, *n* (%)	Strong, *n* (%)	Negative, *n* (%)	Weak, *n* (%)	Strong, *n* (%)
Tumor stage												
Total	65	130	23	66	53	99	29	65	151	15	60	150
pT1-pT2	34 (52.3)	62 (47.7)	8 (34.8)	21 (31.8)	23 (43.4)	60 (60.6)	15 (51.7)	32 (49.2)	69 (45.7)	7 (46.7)	33 (55)	64 (42.7)
pT3-pT4	31 (47.7)	68 (52.3)	15 (65.2)	45 (68.2)	30 (56.6)	39 (39.4)	14 (48.3)	33 (50.8)	82 (54.3)	8 (53.3)	27 (45)	86 (57.3)
P		NS			.0011			NS			NS	
Differentiation grade												
Total	65	130	23	64	53	99	29	65	151	15	60	150
I	24 (36.9)	25 (19.2)	1 (4.3)	5 (7.8)	7 (13.2)	38 (38.4)	3 (10.3)	19 (29.2)	34 (22.5)	1 (6.7)	5 (8.3)	45 (30)
II	29 (44.6)	60 (46.2)	7 (30.4)	23 (35.9)	25 (47.2)	47 (47.5)	9 (31)	27 (41.5)	73 (48.3)	6 (40)	41 (68.3)	50 (33.3)
III	12 (18.5)	45 (34.6)	15 (65.2)	36 (56.2)	21 (39.6)	14 (14.1)	17 (58.6)	19 (29.2)	44 (29.1)	8 (53.3)	14 (23.3)	55 (36.7)
P		.0002			<.0001			.0193			<.0001	
Sarcomatoid differentiation												
Total	65	129	23	66	52	99	29	65	150	15	60	150
Not sarcomatoid	57 (87.7)	91 (70.5)	8 (34.8)	30 (45.5)	38 (73.1)	88 (88.9)	15 (51.7)	45 (69.2)	116 (77.3)	8 (53.3)	49 (81.7)	102 (68)
Sarcomatoid	8 (12.3)	38 (29.5)	15 (65.2)	36 (54.5)	14 (26.9)	11 (11.1)	14 (48.3)	20 (30.8)	34 (22.7)	7 (46.7)	11 (18.3)	48 (32)
P		<.0001			<.0001			.0158			.0453	
Tumor necrosis												
Total	65	130	23	66	53	99	29	65	151	15	60	150
No necrosis	46 (70.7)	81 (62.3)	8 (34.8)	20 (30.3)	30 (56.6)	85 (85.9)	9 (31)	41 (63.1)	105 (69.5)	12 (80)	36 (60)	89 (59.3)
Necrosis	19 (29.2)	49 (37.7)	15 (65.2)	46 (69.7)	23 (43.4)	14 (14.1)	20 (69)	24 (36.9)	46 (30.5)	3 (20)	24 (40)	61 (40.7)
P		.0093			<.0001			.0004			NS	
Lymphocyte infiltration												
Total	65	130	23	66	53	99	29	65	151	15	60	150
Low	16 (24.6)	17 (13.1)	3 (13)	5 (7.6)	5 (9.4)	26 (26.3)	6 (20.7)	18 (27.7)	23 (15.2)	1 (6.7)	5 (8.3)	30 (20)
Moderate	36 (55.4)	68 (52.3	10 (43.5)	26 (39.4)	32 (60.4)	56 (56.6)	12 (41.4)	27 (41.5)	83 (55)	9 (60)	33 (55)	73 (48.7)
Strong	13 (20)	45 (34.6)	10 (43.5)	35 (53)	16 (30.2)	17 (17.2)	11 (37.9)	20 (30.8)	45 (29.8)	5 (33.3)	22 (36.7)	47 (31.3)
P		NS			<.0001			NS			NS	

Statistic evaluation of the correlation between pVHL-dependent cell surface proteins (AXL, CD10, and GLUT-1) and clinicopathologic parameters.
NS indicates not significant.

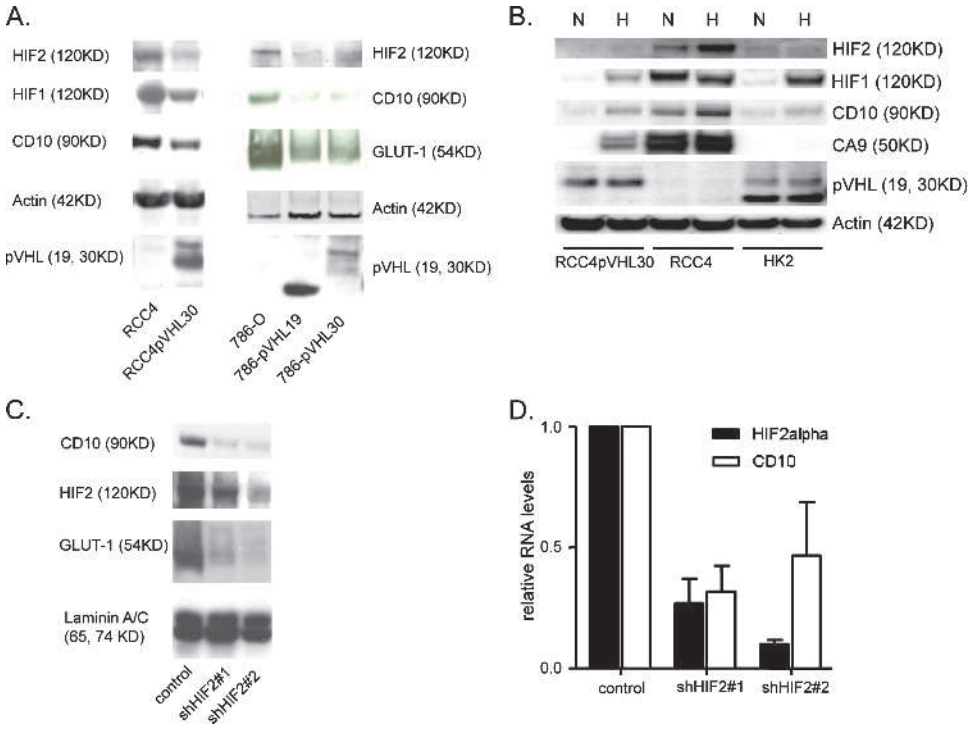

Figure 3. CD10 expression is increased due to pVHL loss-of-function, HIFα stabilization, and hypoxia. (A) Immunoblot analysis of CD10, GLUT-1, HIF-1α, HIF-2α, and pVHL expression in 786-O, 786-O-pVHL$_{19}$, 786-O-pVHL$_{30}$, RCC4, and RCC4pVHL$_{30}$. Actin was used as protein loading control. (B) Immunoblot analysis of CD10, HIF-1α, and HIF-2α expression in RCC4, RCC4-pVHL$_{30}$, and HK-2 under normoxic (N, 20% O_2) or hypoxic (H, 1% O_2) conditions. (C) CD10 expression after silencing of HIF-2α. Western blot analysis of CD10, HIF-2α, and GLUT-1 expression in 786-O with or with no shRNA against HIF-2α. shRNA expression reduces HIF-2α protein levels followed by a decrease of GLUT-1 and CD10. Laminin A/C was used as protein loading control. (D) mRNA expression levels of HIF-2α and CD10 in 786-O–positive or –negative for shRNA against HIF-2α.

We next performed site-directed mutagenesis to confirm the inducibility of the *CD10* promoter by HIF through HREI, which showed the strongest induction of luciferase activity (Figure W1). HK-2 cells transfected with a CD10$_{(-5134/-1005)}$ reporter construct containing a mutated HREI (CD10$_{MUT}$) were cultured under normoxic or hypoxic conditions (Figure 4*C*). Mutagenesis of HREI resulted in a two-fold reduction of luciferase activity under hypoxia. There was no induction of CD10$_{MUT}$ activity under hypoxia compared with normoxia. Hypoxia-induced HIF activity was verified by a six-fold induction of the wild-type P2P reporter construct. This result suggests that HREI is a functional HIF-binding site in the *CD10* promoter and that *CD10* is a bona fide HIF target gene.

A comprehensive TMA analysis of CD10 expression in ccRCC was performed to confirm the regulatory effect of HIF on *CD10* in ccRCC tissue. Three TMAs containing 831 ccRCCs were analyzed for membrane staining of CD10 and the HIF targets CAIX, GLUT-1, and CCND1. CD10 expression correlated significantly with CAIX, GLUT-1 ($P < .0001$, each), and CCND1 ($P = .0005$). Because HIF suppresses *E-cadherin* gene transcription, E-cadherin expression was also analyzed. We found an inverse correlation between E-cadherin–negative and CD10-positive tumors ($P < .0001$). No correlation was found between CD10, CAIX, or GLUT-1 expression and survival.

CD10 Inhibition Reduces the Invasive Behavior of Renal Carcinoma Cells

The effect of CD10 on the invasive behavior of ccRCC cells was determined using cell invasion assays. For this purpose, 786-O and 786-OpVHL$_{30}$ were seeded on a reconstituted basement membrane matrix in the presence or absence of the specific CD10 inhibitor thiorphan. The highly invasive fibrosarcoma cell line HT-1080 was used as a positive (with 10% FCS in the lower chamber) or a negative (without FCS in the lower chamber) control. 786-O cells, which express high levels of CD10, showed a 1.6-fold enhanced invasive potential compared with 786-OpVHL$_{30}$ cells (Figure 4*D*). A 1.9- and 2.3-fold decrease of cell invasion was measured after addition of the CD10-specific inhibitor thiorphan to 786-O and 786-OpVHL$_{30}$ cells, respectively. Notably, in the presence of pVHL, 1 μM thiorphan was sufficient to decrease the invasive potential of the tumor cells. In contrast, in VHL-negative 786-O, a 10-fold dose (10 μM) of thiorphan was needed to yield the same effect.

Detection of CD10 in the Serum of RCC Patients

Identification of serum biomarkers for diagnosis, prognosis, or disease progression monitoring of ccRCC represents an ultimate goal in renal cancer research. We analyzed thus the potential of CD10 as ccRCC-associated serum biomarker. CD10 is frequently expressed in tissue, but its potentially elevated abundance in sera from patients with ccRCC is unknown [38–40]. Therefore, sera from ccRCC patients ($n = 15$), patients with other renal carcinoma subtypes ($n = 6$), and normal healthy controls ($n = 8$) were analyzed using a commercial CD10-specific ELISA. The analysis showed that the CD10 serum protein concentration was significantly increased in a subset of ccRCC patients (494.3 ± 125.8 pg/ml) compared with healthy individuals (173.7 ± 43.99 pg/ml, $P = .01$). Patients diagnosed

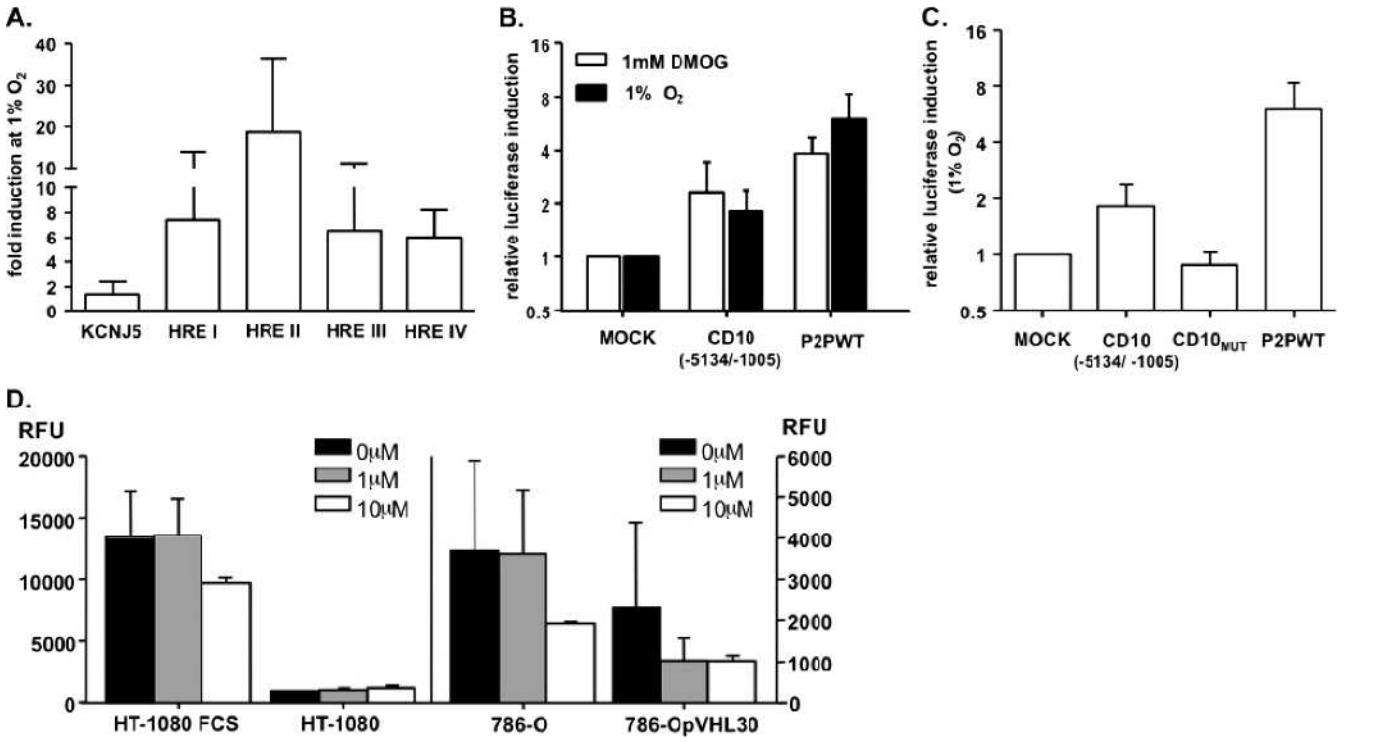

Figure 4. HIF-1α binds and activates the *CD10* promoter, resulting in increased CD10-dependent tumor cell invasion. (A) Binding of HIF-1α at the *CD10* promoter analyzed by ChIP. HREI-IV indicates *in silico* identified HRE elements in the *CD10* promoter; *KCNJ5*, negative control. Experiments were performed in HEK-293 cells grown in normoxia or hypoxia. Results are shown as ratios of the amplicons detected under hypoxia *versus* normoxia. (B) Luciferase reporter gene assay. Relative luciferase gene expression differences of a reporter construct containing a 4-kb 5′ region flanking *CD10* in HK-2 cells treated with hypoxia or DMOG normalized to untreated cells. A cotransfected renilla luciferase expression vector was used for normalization of transfection efficiency. P2PWT served as positive control for HIF activity. Data are expressed as mean ± SDs. (C) Relative luciferase activity of a reporter construct containing wild-type or mutated HREI of *CD10* after hypoxic treatment of HK-2 cells. Values are normalized to HK-2 cultured under normoxia. A cotransfected renilla luciferase expression vector was used for normalization of transfection efficiency. P2PWT served as a positive control for HIF activity. Data are expressed as mean ± SDs. (D) Inhibition of CD10 by thiorphan reduces the invasive potential of 786-O cells. Invasion of 786-O and 786-OpVHL$_{30}$ cells through a biomatrix was quantified fluorometrically in the absence or presence of the indicated concentrations of thiorphan. Data are expressed as mean ± SDs. RFU indicates relative fluorescence unit.

with other renal carcinoma subtypes without *VHL* alterations had CD10 levels comparable to healthy controls (117.4 ± 25.32 pg/ml; Figure 5). This result indicates that CD10 may be useful as a potential serum biomarker for the detection of recurrent ccRCC after nephrectomy or preoperative treatment stratification of RCC patients based on the tumor subtype.

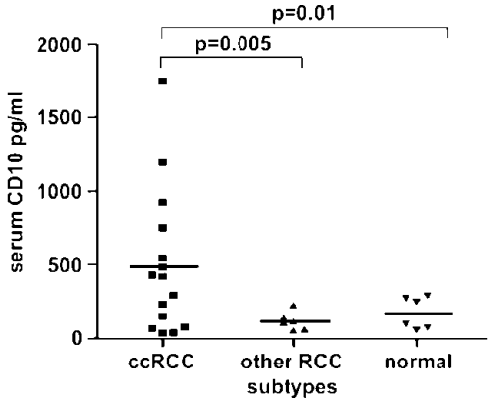

Figure 5. Abundance of CD10 in human RCC samples. CD10 serum levels in ccRCC patients (n = 15), other RCC subtypes (n = 6), and healthy controls (n = 6) measured by ELISA.

Discussion

Reliable and specific cell surface protein markers for the early detection of most cancer types are still lacking. Discovery-driven approaches thus attempt to identify tumor-specific protein markers, which are cell surface accessible for drug targeting, or detectable in body fluids, for example, serum, plasma, or urine, for noninvasive diagnostic analysis. During the last few years, LC-MS/MS–based proteomics became a powerful technology capable of addressing the needs of the clinical community for biomarker discovery on the protein level. Here, CSC-based proteomic technology was used for an initial screen toward the identification of potential cell surface glycoprotein targets in the context of *VHL* inactivation in ccRCC. The screening data were validated through transcriptomic, immunohistochemical, as well as functional assays.

Using a ccRCC-derived model of pVHL-positive and pVHL-negative cells, we screened for N-glyco-cell surface–exposed proteins. This initial screen revealed ccRCC-expressed cell surface glycoproteins including their specific cotranslational N-glycosylation sites. In contrast to antibody-dependent strategies for cell surface protein identification,

we could identify ccRCC glycoproteins through their N-glycosites using the complementary CSC technology for which no commercial antibodies are currently available. These cell surface–exposed glycoproteins and potential diagnostic markers are currently invisible for antibody-based phenotyping strategies. The combination of the CSC technology with relative SILAC-based quantification of the surfaceome in the context of pVHL expression enabled us to detect potential changes in the protein expression pattern within the detected pool of RCC glycoproteins. These relative quantitative changes of glycoproteins in the cell surface location render the cells' capabilities to communicate with the microenvironment, limiting or enhancing signaling capacities. We were also able to further subdivide the cell surface proteome into pVHL-dependent and nonassociated pathways. A clear separation into pVHL-dependent and pVHL-independent pathways may improve the efficiency and decrease unwanted adverse effects of future therapeutic strategies. Our initial proteomic screening results suggested that, besides known pVHL-dependent pathways (e.g., inflammation, MAPK, cadherin signaling), additional signaling pathways such as the endothelin pathway contribute to ccRCC carcinogenesis [41].

Our screen of the surfaceome indicated CD10 and AXL as pVHL-regulated cell surface proteins. The molecular mechanism of the cell surface metalloproteinase CD10 regulation in ccRCC was so far unknown. Previous studies have reported variable expression of CD10 in human sporadic ccRCC [38,39,42]. Here we demonstrate that the activation of *CD10* is directly regulated through HIF, which occurs as a consequence of loss of pVHL function in ccRCC. In addition, cell invasion assays implicate CD10 in ccRCC progression potentially linked to increased invasive behavior. Indeed, inhibition of CD10 by the specific inhibitor thiorphan resulted in a reduced invasive behavior of tumor cells. Interestingly, pVHL-expressing tumor cells were more sensitive to lower amounts of thiorphan than pVHL-negative tumor cells. The therapeutic efficiency of CD10 inhibitors may thus depend on the *VHL* mutation status in ccRCC patients.

Serum assays, enabling early diagnosis of ccRCC patients are currently lacking. Shedding and accumulation of tumor-specific cell surface proteins, such as CD10, in the body fluids exploited for novel ELISA-based strategies would allow earlier diagnosis of primary tumors or metastasis occurring after nephrectomy, resulting in improved prognosis of ccRCC. On the basis of our proteomic results and the hypothesis that proteins such as the cell surface protein CD10 might also be shed in the serum, we established and tested an ELISA to analyze the serum protein levels of CD10. This analysis revealed a significantly higher CD10 serum level in VHL-related ccRCC compared with normal controls and non–VHL-related RCC subtypes, for example, papillary RCC (pRCC). Therefore, CD10 may represent a promising serum marker for ccRCC, which is potentially useful to screen patients after RCC-related nephrectomy for the development of metastases.

The second interesting candidate, which was discovered in our relative quantitative experiments, was the receptor tyrosine kinase AXL. AXL was recently highlighted as a therapeutic target in pancreatic and lung adenocarcinoma [43,44]. Our immunohistochemical analysis demonstrated that AXL is also expressed in ccRCC cells as well as in endothelial cells. There was a significant correlation between high number of AXL-positive endothelial cells and better patient's outcome. This finding correlates with the data of previous studies, which showed an association between high microvessel density in ccRCC measured by the endothelial marker CD34 and better patient's outcome [45,46]. In contrast, strong epithelial AXL expression is related to parameters of poor prognosis, for example, high nuclear differentiation grade, presence of necrosis, and sarcomatoid differentiation. This is consistent with the recently reported data confirming that epithelial AXL expression is an indicator of tumor progression in pancreatic cancer, glioblastoma, drug-resistant myeloid leukemia, and non–small cell lung cancer [43,47]. Very recently, AXL mRNA and serum protein levels were shown to correlate with poor patient prognosis in RCC, but the exact cellular protein expression pattern was not studied [47]. This recent identification of AXL the in serum of RCC patients demonstrates that our SILAC CSC strategy was able to identify, in addition to CD10, a second ccRCC-specific member of the N-glyco-cell surface subproteome, which is also shed into bloodstream circulation.

In summary, our proteotranscriptomic screening identified novel pVHL and HIF-dependent components, which may represent the basis for novel molecular targeted therapies and diagnostic strategies in ccRCC. Among a number of interesting candidates, we characterized in-depth *CD10* as a HIF target gene and show that its inhibition leads to a less invasive phenotype of ccRCC cells. Furthermore, CD10 and AXL may be promising biomarker candidates for the identification of ccRCC in serum samples. Further analysis of the pVHL-dependent surfaceome may thus help to improve current therapeutic applications toward a more personalized tumor-specific treatment.

Acknowledgments

The authors thank Susanne Dettwiler, Martina Storz, Silvia Behnke, Roger Santimaria, and Kirsten Struckmann for their excellent technical support; Lukas John Hefermehl and Stefanie Dannenmann for collecting and providing RCC patients sera; and Manfred Beleut and Carolina B. Ferreira for their critical suggestions on the article.

References

[1] Chen J, Kobayashi M, Darmanin S, Qiao Y, Gully C, Zhao R, Yeung SC, and Lee MH (2009). Pim-1 plays a pivotal role in hypoxia-induced chemoresistance. *Oncogene* **28**, 2581–2592.

[2] Gatenby RA, Kessler HB, Rosenblum JS, Coia LR, Moldofsky PJ, Hartz WH, and Broder GJ (1988). Oxygen distribution in squamous cell carcinoma metastases and its relationship to outcome of radiation therapy. *Int J Radiat Oncol Biol Phys* **14**, 831–838.

[3] Teicher BA, Lazo JS, and Sartorelli AC (1981). Classification of antineoplastic agents by their selective toxicities toward oxygenated and hypoxic tumor cells. *Cancer Res* **41**, 73–81.

[4] Toffoli S and Michiels C (2008). Intermittent hypoxia is a key regulator of cancer cell and endothelial cell interplay in tumours. *FEBS J* **275**, 2991–3002.

[5] Motzer RJ, Hutson TE, Tomczak P, Michaelson MD, Bukowski RM, Rixe O, Oudard S, Negrier S, Szczylik C, Kim ST, et al. (2007). Sunitinib *versus* interferon alfa in metastatic renal-cell carcinoma. *N Engl J Med* **356**, 115–124.

[6] Motzer RJ, Michaelson MD, Rosenberg J, Bukowski RM, Curti BD, George DJ, Hudes GR, Redman BG, Margolin KA, and Wilding G (2007). Sunitinib efficacy against advanced renal cell carcinoma. *J Urol* **178**, 1883–1887.

[7] Escudier B, Lassau N, Angevin E, Soria JC, Chami L, Lamuraglia M, Zafarana E, Landreau V, Schwartz B, Brendel E, et al. (2007). Phase I trial of sorafenib in combination with IFN α-2a in patients with unresectable and/or metastatic renal cell carcinoma or malignant melanoma. *Clin Cancer Res* **13**, 1801–1809.

[8] Motzer RJ, Rini BI, Bukowski RM, Curti BD, George DJ, Hudes GR, Redman BG, Margolin KA, Merchan JR, Wilding G, et al. (2006). Sunitinib in patients with metastatic renal cell carcinoma. *JAMA* **295**, 2516–2524.

[9] Hood BL, Malehorn DE, Conrads TP, and Bigbee WL (2009). Serum proteomics using mass spectrometry. *Methods Mol Biol* **520**, 107–128.

[10] Wollscheid B, Bausch-Fluck D, Henderson C, O'Brien R, Bibel M, Schiess R, Aebersold R, and Watts JD (2009). Mass-spectrometric identification and relative quantification of N-linked cell surface glycoproteins. *Nat Biotechnol* **27**, 378–386.

[11] Schiess R, Wollscheid B, and Aebersold R (2009). Targeted proteomic strategy for clinical biomarker discovery. *Mol Oncol* **3**, 33–44.

[12] Luu VD, Fischer B, von Teichman A, Boysen G, Mertz K, Zimmermann P, Moch H, and Schraml P (2008). Von-Hippel–Lindau gene mutation types. Association of gene expression signatures in clear cell renal cell carcinoma [in German]. *Pathologe* **29**(suppl 2), 303–307.

[13] Banks RE, Tirukonda P, Taylor C, Hornigold N, Astuti D, Cohen D, Maher ER, Stanley AJ, Harnden P, Joyce A, et al. (2006). Genetic and epigenetic analysis of von Hippel–Lindau (VHL) gene alterations and relationship with clinical variables in sporadic renal cancer. *Cancer Res* **66**, 2000–2011.

[14] van Houwelingen KP, van Dijk BA, Hulsbergen-van de Kaa CA, Schouten LJ, Gorissen HJ, Schalken JA, van den Brandt PA, and Oosterwijk E (2005). Prevalence of von Hippel–Lindau gene mutations in sporadic renal cell carcinoma: results from The Netherlands cohort study. *BMC Cancer* **5**, 57.

[15] Herman JG, Latif F, Weng Y, Lerman MI, Zbar B, Liu S, Samid D, Duan DS, Gnarra JR, Linehan WM, et al. (1994). Silencing of the VHL tumor-suppressor gene by DNA methylation in renal carcinoma. *Proc Natl Acad Sci USA* **91**, 9700–9704.

[16] Rechsteiner MP, von Teichman A, Nowicka A, Sulser T, Schraml P, and Moch H (2011). VHL gene mutations and their effects on hypoxia inducible factor HIFα: identification of potential driver and passenger mutations. *Cancer Res* **71**, 5500–5511.

[17] Iliopoulos O, Ohh M, and Kaelin WG Jr (1998). $pVHL_{19}$ is a biologically active product of the von Hippel–Lindau gene arising from internal translation initiation. *Proc Natl Acad Sci USA* **95**, 11661–11666.

[18] Schraml P, Hergovich A, Hatz F, Amin MB, Lim SD, Krek W, Mihatsch MJ, and Moch H (2003). Relevance of nuclear and cytoplasmic von Hippel–Lindau protein expression for renal carcinoma progression. *Am J Pathol* **163**, 1013–1020.

[19] Hergovich A, Lisztwan J, Barry R, Ballschmieter P, and Krek W (2003). Regulation of microtubule stability by the von Hippel–Lindau tumour suppressor protein pVHL. *Nat Cell Biol* **5**, 64–70.

[20] Lisztwan J, Imbert G, Wirbelauer C, Gstaiger M, and Krek W (1999). The von Hippel–Lindau tumor suppressor protein is a component of an E3 ubiquitin-protein ligase activity. *Genes Dev* **13**, 1822–1833.

[21] Maxwell PH, Wiesener MS, Chang GW, Clifford SC, Vaux EC, Cockman ME, Wykoff CC, Pugh CW, Maher ER, and Ratcliffe PJ (1999). The tumour suppressor protein VHL targets hypoxia-inducible factors for oxygen-dependent proteolysis. *Nature* **399**, 271–275.

[22] Min JH, Yang H, Ivan M, Gertler F, Kaelin WG Jr, and Pavletich NP (2002). Structure of an HIF-1α –pVHL complex: hydroxyproline recognition in signaling. *Science* **296**, 1886–1889.

[23] Ivan M, Kondo K, Yang H, Kim W, Valiando J, Ohh M, Salic A, Asara JM, Lane WS, and Kaelin WG Jr (2001). HIFα targeted for VHL-mediated destruction by proline hydroxylation: implications for O_2 sensing. *Science* **292**, 464–468.

[24] Kaelin WG Jr (2007). The von Hippel–Lindau tumor suppressor protein and clear cell renal carcinoma. *Clin Cancer Res* **13**, 680s–684s.

[25] Hergovich A, Lisztwan J, Thoma CR, Wirbelauer C, Barry RE, and Krek W (2006). Priming-dependent phosphorylation and regulation of the tumor suppressor pVHL by glycogen synthase kinase 3. *Mol Cell Biol* **26**, 5784–5796.

[26] Thoma CR, Frew IJ, Hoerner CR, Montani M, Moch H, and Krek W (2007). pVHL and GSK3β are components of a primary cilium—maintenance signalling network. *Nat Cell Biol* **9**, 588–595.

[27] Li XJ, Zhang H, Ranish JA, and Aebersold R (2003). Automated statistical analysis of protein abundance ratios from data generated by stable-isotope dilution and tandem mass spectrometry. *Anal Chem* **75**, 6648–6657.

[28] Kononen J, Bubendorf L, Kallioniemi A, Barlund M, Schraml P, Leighton S, Torhorst J, Mihatsch MJ, Sauter G, and Kallioniemi OP (1998). Tissue microarrays for high-throughput molecular profiling of tumor specimens. *Nat Med* **4**, 844–847.

[29] Dahinden C, Ingold B, Wild P, Boysen G, Luu VD, Montani M, Kristiansen G, Sulser T, Buhlmann P, Moch H, et al. (2010). Mining tissue microarray data to uncover combinations of biomarker expression patterns that improve intermediate staging and grading of clear cell renal cell cancer. *Clin Cancer Res* **16**, 88–98.

[30] Metzen E, Stiehl DP, Doege K, Marxsen JH, Hellwig-Burgel T, and Jelkmann W (2005). Regulation of the prolyl hydroxylase domain protein 2 (*phd2/egln-1*) gene: identification of a functional hypoxia-responsive element. *Biochem J* **387**, 711–717.

[31] Suzuki R and Shimodaira H (2006). Pvclust: an R package for assessing the uncertainty in hierarchical clustering. *Bioinformatics* **22**, 1540–1542.

[32] Team RDC (2008). *R: A Language and Environment for Statistical Computing*. R Foundation for Statistical Computing, Vienna, Austria.

[33] Liaw A and Wiener M (2002). Classification and regression by random forest. *R News* **2**, 18–22.

[34] Ishimaru F and Shipp MA (1995). Analysis of the human CD10/neutral endopeptidase 24.11 promoter region: two separate regulatory elements. *Blood* **85**, 3199–3207.

[35] Haouas H, Morello D, Lavenu A, Billard M, Jasmin C, and Boucheix C (1995). Characterization of the 5′ region of the CD10/neutral endopeptidase 24.11 gene. *Biochem Biophys Res Commun* **207**, 933–942.

[36] Sezaki N, Ishimaru F, Tabayashi T, Kataoka I, Nakase K, Fujii K, Kozuka T, Nakayama H, Harada M, and Tanimoto M (2003). The type 1 CD10/neutral endopeptidase 24.11 promoter: functional characterization of the 5′-untranslated region. *Br J Haematol* **123**, 177–183.

[37] Wenger RH, Stiehl DP, and Camenisch G (2005). Integration of oxygen signaling at the consensus HRE. *Sci STKE* **2005**, re12.

[38] Langner C, Ratschek M, Rehak P, Schips L, and Zigeuner R (2004). CD10 is a diagnostic and prognostic marker in renal malignancies. *Histopathology* **45**, 460–467.

[39] Chu P and Arber DA (2000). Paraffin-section detection of CD10 in 505 nonhematopoietic neoplasms. Frequent expression in renal cell carcinoma and endometrial stromal sarcoma. *Am J Clin Pathol* **113**, 374–382.

[40] Butnor KJ, Nicholson AG, Allred DC, Zander DS, Henderson DW, Barrios R, Haque AK, Allen TC, Killen DE, and Cagle PT (2006). Expression of renal cell carcinoma–associated markers erythropoietin, CD10, and renal cell carcinoma marker in diffuse malignant mesothelioma and metastatic renal cell carcinoma. *Arch Pathol Lab Med* **130**, 823–827.

[41] Gordan JD, Lal P, Dondeti VR, Letrero R, Parekh KN, Oquendo CE, Greenberg RA, Flaherty KT, Rathmell WK, Keith B, et al. (2008). HIF-α effects on c-Myc distinguish two subtypes of sporadic VHL-deficient clear cell renal carcinoma. *Cancer Cell* **14**, 435–446.

[42] Avery AK, Beckstead J, Renshaw AA, and Corless CL (2000). Use of antibodies to RCC and CD10 in the differential diagnosis of renal neoplasms. *Am J Surg Pathol* **24**, 203–210.

[43] Koorstra JB, Karikari CA, Feldmann G, Bisht S, Rojas PL, Offerhaus GJ, Alvarez H, and Maitra A (2009). The Axl receptor tyrosine kinase confers an adverse prognostic influence in pancreatic cancer and represents a new therapeutic target. *Cancer Biol Ther* **8**, 618–626.

[44] Lay JD, Hong CC, Huang JS, Yang YY, Pao CY, Liu CH, Lai YP, Lai GM, Cheng AL, Su IJ, et al. (2007). Sulfasalazine suppresses drug resistance and invasiveness of lung adenocarcinoma cells expressing AXL. *Cancer Res* **67**, 3878–3887.

[45] Mertz KD, Demichelis F, Kim R, Schraml P, Storz M, Diener PA, Moch H, and Rubin MA (2007). Automated immunofluorescence analysis defines microvessel area as a prognostic parameter in clear cell renal cell cancer. *Hum Pathol* **38**, 1454–1462.

[46] Schraml P, Struckmann K, Hatz F, Sonnet S, Kully C, Gasser T, Sauter G, Mihatsch MJ, and Moch H (2002). VHL mutations and their correlation with tumour cell proliferation, microvessel density, and patient prognosis in clear cell renal cell carcinoma. *J Pathol* **196**, 186–193.

[47] Gustafsson A, Martuszewska D, Johansson M, Ekman C, Hafizi S, Ljungberg B, and Dahlback B (2009). Differential expression of Axl and Gas6 in renal cell carcinoma reflecting tumor advancement and survival. *Clin Cancer Res* **15**, 4742–4749.

Table W4. List of All SILAC-CSC Experiments Used for the Initial Screen Including the Number of LC-MS/MS Runs.

Experiment No.	Description	Replicates	Mass Spectrometer	No. LC-MS/MS Runs	Data Set(s)
1	SILAC CSC; 786-O light, 786-3O heavy labeled	wt/30 replicate 1	hybrid LTQ-FT (Thermo Fisher Scientific)	2	B06-12037_gb5_30-1, B06-12038_gb5_30-2
2	SILAC CSC; 786-O light, 786-O heavy labeled	control replicate 1	hybrid LTQ-FT (Thermo Fisher Scientific)	2	B06-12039_db5_wt1, B06-12040_gb5_wt2

Listed are the two different experimental settings with a description, an annotation of the replicates, the corresponding number of LC-MS/MS runs, and the mass spectrometer used for the analysis of the sample.

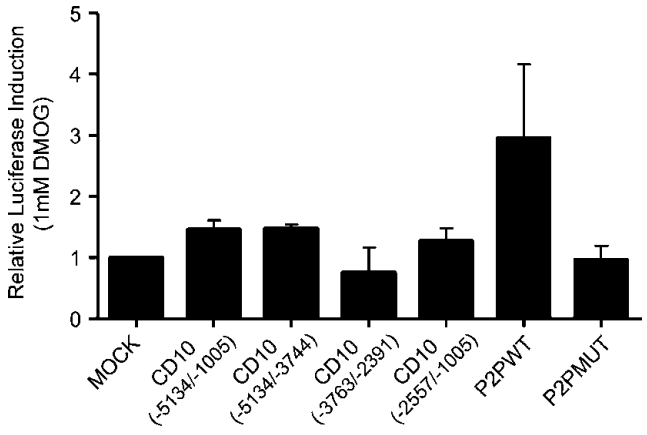

Figure W1. Relative induction of the luciferase activity of CD10 reporter constructs containing the individual HRE. HEK-293 cells were treated with or without DMOG. Whole-cell lysates were used for luciferase assay. A cotransfected renilla luciferase expression vector was used for normalization of transfection efficiency. P2PWT and P2PMUT served as positive and negative control for HIF activity. Data are expressed as mean ± SDs.

Table W5. List of Screened Proteins that Were Quantified by Using SILAC CSC.

No. Proteins	Name	IPI	Entrez	786-O/ 786-OpVHL$_{30}$	Ratio –O/–30 SD
1	ABCB1	IPI00027481	5243	NA	NA
2	ADAM10	IPI00013897	102	NA	NA
3	**ADCY9**	**IPI00030099**	**115**	**0.02**	**0.01**
4	ALCAM	IPI00015102	214	1.36	2.08
5	ANO6	IPI00151710	196527	NA	NA
6	ANPEP	IPI00221224	290	0.64	0.35
7	ASAM	IPI00024929	79827	0.57	0.43
8	ATP1B1	IPI00179529	481	NA	NA
9	ATP1B3	IPI00008167	483	2.03	0.79
10	**AXL**	**IPI00296992**	**558**	**0.27**	**0.32**
11	BCAM	IPI00002406	4059	1.21	0.46
12	BSG	IPI00019906	682	1.10	1.60
13	BST2	IPI00026241	684	1.74	1.06
14	C1QTNF3	IPI00166261	114899	NA	NA
15	CA12	IPI00012895	771	NA	NA
16	CADM1	IPI00003813	23705	1.12	1.90
17	CD109	IPI00152540	135228	2.61	1.33
18	CD276	IPI00019275	80381	1.37	1.56
19	CD40	IPI00018282	958	NA	NA
20	**CD44**	**IPI00002541**	**960**	**0.23**	**0.31**
21	CD47	IPI00216516	961	NA	NA
22	CD63	IPI00215998	967	NA	NA
23	CD70	IPI00031713	970	0.42	0.60
24	CD82	IPI00020446	3732	0.70	0.27
25	CD97	IPI00299412	976	2.68	2.18
26	CDCP1	IPI00290039	64866	1.91	0.96
27	CDH13	IPI00024046	1012	0.36	0.52
28	CDH2	IPI00290085	1000	0.88	0.98
29	CDH6	IPI00024035	1004	1.27	0.46
30	CLDND1	IPI00072743	56650	1.93	1.27
31	DPP4	IPI00018953	1803	0.87	0.32
32	**DSG2**	**IPI00028931**	**1829**	**0.15**	**0.05**
33	ECE1	IPI00002478	1889	0.93	0.34
34	**EGFR**	**IPI00018274**	**1956**	**0.21**	**0.34**
35	ELFN2	IPI00289849	114794	0.48	0.16
36	**ENPEP**	**IPI00014375**	**2028**	**0.18**	**0.18**
37	EPHA2	IPI00021267	1969	0.72	0.35
38	**F3**	**IPI00010338**	**2152**	**0.22**	**0.14**
39	FN1	IPI00022418	2335	NA	NA
40	GFRA1	IPI00008148	2674	1.42	0.51
41	GGT1	IPI00018901	2678	NA	NA
42	GGT2	IPI00002241	728441	NA	NA
43	GPC1	IPI00015688	2817	NA	NA
44	GPR126	IPI00217481	57211	NA	NA
45	HEG	IPI00297263	57493	NA	NA
46	HLA-B	IPI00004657	3106	NA	NA
47	HSPG2	IPI00024284	3339	NA	NA
48	ICAM1	IPI00008494	3383	1.02	0.98
49	ITFG3	IPI00396658	83986	NA	NA
50	**ITGA1**	**IPI00472202**	**3672**	**0.21**	**0.08**
51	ITGA2	IPI00013744	3673	NA	NA
52	ITGA3	IPI00215995	3675	0.56	0.46
53	ITGA5	IPI00306604	3678	2.78	1.19
54	ITGAV	IPI00027505	3685	1.14	1.60
55	KIAA1549	IPI00397393	57670	NA	NA
56	KIRREL	IPI00470360	55243	NA	NA
57	**LTBR**	**IPI00006097**	**4055**	**0.25**	**0.09**
58	M6PR	IPI00025049	4074	NA	NA
59	MCAM	IPI00016334	4162	NA	NA
60	**MICA**	**IPI00107380**	**3106**	**0.22**	**0.08**
61	MME	IPI00247063	4311	NA	NA
62	MPZL1	IPI00022558	9019	NA	NA
63	MRC2	IPI00005707	9902	NA	NA
64	NCAM1	IPI00185362	4684	NA	NA
65	NCSTN	IPI00021983	23385	NA	NA
66	**NPTN**	**IPI00011578**	**27020**	**0.12**	**0.05**
67	NRP1	IPI00165438	8829	NA	NA
68	NRP2	IPI00029693	8828	NA	NA
69	NT5E	IPI00009456	4907	1.18	0.61
70	OSMR	IPI00022674	9180	NA	NA
71	PLXNB2	IPI00398435	23654	0.36	0.29
72	PON1	IPI00218732	5444	NA	NA
73	PRNP	IPI00022284	5621	0.46	0.43
74	PROCR	IPI00009276	10544	NA	NA
75	PTGFRN	IPI00022048	5738	0.38	0.42
76	PTPRF	IPI00107831	5792	2.88	3.27
77	PTPRJ	IPI00290328	5795	0.70	0.29
78	**PTPRK**	**IPI00015756**	**5796**	**0.19**	**0.08**
79	PVR	IPI00219425	5817	NA	NA
80	**PVRL1**	**IPI00003648**	**5818**	**0.19**	**0.04**
81	SCARB1	IPI00177968	949	0.38	0.15
82	SEMA4B	IPI00419724	10509	NA	NA
83	SERPINF1	IPI00006114	5176	0.59	0.23
84	**SIRPA**	**IPI00332887**	**140885**	**12.15**	**4.20**
85	**SLC19A1**	**IPI00375452**	**6573**	**16.08**	**5.56**
86	SLC1A4	IPI00015476	6509	1.15	0.64
87	SLC22A4	IPI00171334	6583	1.52	0.52
88	**SLC29A1**	**IPI00550382**	**2030**	**0.19**	**0.24**
89	**SLC2A1**	**IPI00220194**	**6513**	**5.54**	**2.32**
90	**SLC39A14**	**IPI00014236**	**23516**	**0.12**	**0.07**
91	**SLC39A6**	**IPI00298702**	**25800**	**0.08**	**0.03**
92	SLC3A2	IPI00027493	6520	0.36	0.76
93	SLC44A2	IPI00293074	57153	NA	NA
94	SLC4A7	IPI00021058	9497	NA	NA
95	SLC6A6	IPI00216143	6533	NA	NA
96	**SLC7A1**	**IPI00027728**	**6541**	**3.76**	**5.03**
97	**THBS1**	**IPI00296099**	**7057**	**7.56**	**3.36**
98	**TMEM2**	**IPI00170706**	**23670**	**0.27**	**0.10**
99	TMEM30A	IPI00019381	55754	NA	NA
100	**TNC**	**IPI00031008**	**3371**	**0.33**	**0.45**
101	TPBG	IPI00009111	7162	1.71	2.76
102	TSHB	IPI00000851	7252	NA	NA
103	URB	IPI00260630	151887	NA	NA
104	VASN	IPI00395488	114990	NA	NA
105	VCAM1	IPI00018136	7412	1.14	1.19
106	VCAN	IPI00009802	1462	NA	NA

Shown is the list of 106 proteins identified with at least one peptide containing the NXS/T consensus glycosylation motif. Displayed columns are the protein number, gene name, IPI identifier, Entrez number, ASAP ratios, SD, and number of peptides used for quantitation from experiments 1 and 2 (Table W4). The shown ratios are L/H. A total of 63 proteins could be quantified. Differentially expressed proteins are marked **bold**.

Table W6. List of 23 pVHL-Dependent Cell Surface Glycoproteins Detected in ccRCC Cells.

No. Proteins	Name	IPI	Entrez
1	ADCY9	IPI00009456	115
2	AXL	IPI00296992	558
3	CD44	IPI00002541	960
4	DSG2	IPI00028931	1829
5	EGFR	IPI00018274	1956
6	ENPEP	IPI00014375	2028
7	F3	IPI00010338	2152
8	ITGA1	IPI00743104	3672
9	LTBR	IPI00006097	4055
10	MICA	IPI00107380	3106
11	NPTN	IPI00011578	27020
12	PTPRK	IPI00470937	5796
13	PVRL1	IPI00003648	5818
14	SIRPA	IPI00332887	140885
15	SLC19A1	IPI00375452	6573
16	SLC29A1	IPI00939219	2030
17	SLC2A1	IPI00220194	6513
18	SLC39A14	IPI00014236	23516
19	SLC39A6	IPI00298702	25800
20	SLC7A1	IPI00027728	6541
21	THBS1	IPI00296099	7057
22	TMEM2	IPI00170706	23670
23	TNC	IPI00031008	3371

Listed are the protein number, protein name, IPI number, and Entrez number. The 23 proteins were differently expressed between 786-O and 786-OpVHL$_{30}$.

Table W7. List of 82 Candidates Analyzed for mRNA Expression by Using Customized LDAs.

Number	Gene Name	Entrez Gene ID	RNA 786-O/ 786-OpVHL$_{30}$	Protein 786-O/ 786-OpVHL$_{30}$
1	**F3**	**2152**	**11.11**	**0.22**
2	**SLC1A4**	**6509**	**4.17**	**1.15**
3	**MME**	**4311**	**3.70**	**NA**
4	**ITGA2**	**3673**	**3.03**	**NA**
5	**SLC2A1**	**6513**	**2.94**	**5.54**
6	**NT5E**	**4907**	**2.56**	**1.18**
7	**SLC29A1**	**2030**	**2.50**	**0.19**
8	**CCDC80**	**151887**	**2.27**	**NA**
9	**SLC22A4**	**6583**	**2.22**	**1.52**
10	**SEMA4B**	**10509**	**2.13**	**NA**
11	**CDH2**	**1000**	**2.04**	**0.88**
12	**MRC2**	**9902**	**2.00**	**NA**
13	**SLC39A14**	**23516**	**1.89**	**0.12**
14	**PRNP**	**5621**	**1.85**	**0.46**
15	**HEG1**	**57493**	**1.82**	**NA**
16	**AXL**	**558**	**1.75**	**0.27**
17	ANPEP	290	1.72	0.64
18	CDH13	1012	1.72	0.36
19	GPC1	2817	1.67	NA
20	CA12	771	1.64	NA
21	SLC3A2	6520	1.64	0.36
22	ICAM1	3383	1.56	1.02
23	ITGA5	3678	1.54	2.78
24	ALCAM	214	1.52	1.36
25	KIRREL	55243	1.52	NA
26	SLC7A1	6541	1.52	3.76
27	TNC	3371	1.45	0.33
28	TPBG	7162	1.45	1.71
29	ABCB1	5243	1.43	NA
30	ITGA1	3672	1.43	0.21
31	NCAM1	4684	1.43	NA
32	THBS1	7057	1.43	7.56
33	ATP1B1	481	1.41	NA
34	ADAM10	102	1.39	NA
35	GFRA1	2674	1.35	1.42
36	PTPRF	5792	1.35	2.88
37	SCARB1	949	1.35	0.38
38	CLDND1	56650	1.33	1.93
39	SLC44A2	57153	1.32	NA
40	SLC6A6	6533	1.32	NA
41	SLC39A6	25800	1.28	0.08
42	SLC4A7	9497	1.28	NA
43	EGFR	1956	1.27	0.21
44	CD109	135228	1.23	2.61
45	ITGA3	3675	1.20	0.56
46	PTPRK	5796	1.20	0.19
47	TMEM30A	55754	1.20	NA
48	TMEM2	23670	1.16	0.27
49	NCSTN	23385	1.15	NA
50	OSMR	9180	1.15	NA
51	CD63	967	1.10	NA
52	BST2	684	1.09	1.74
53	MPZL1	9019	1.09	NA
54	BSG	682	1.08	1.10
55	HLA-B	3106	1.08	NA
56	ITFG3	83986	1.06	NA
57	NPTN	27020	1.04	0.12
58	EPHA2	1969	0.99	0.72
59	PLXNB2	23654	0.99	0.36
60	ECE1	1889	0.96	0.93
61	HSPG2	3339	0.96	NA
62	CD276	80381	0.94	1.37
63	CDCP1	64866	0.94	1.91
64	NRP1	8829	0.90	NA
65	PROCR	10544	0.90	NA
66	ENPEP	2028	0.88	0.18
67	CD47	961	0.86	NA
68	GPR126	57211	0.86	NA
69	CD97	976	0.83	2.68
70	ADCY9	115	0.80	0.02
71	DSG2	1829	0.80	0.15
72	LTBR	4055	0.78	0.25
73	PTPRJ	5795	0.78	0.70
74	CD40	958	0.78	NA
75	CD44	960	0.70	NA
76	M6PR	4074	0.70	NA
77	VCAM1	7412	0.68	1.14
78	CD82	3732	0.67	0.70
79	MCAM	4162	0.63	NA
80	**DPP4**	**1803**	**0.53**	**0.87**
81	**CDH6**	**1004**	**0.37**	**1.27**
82	**BCAM**	**4059**	**0.23**	**1.21**

pVHL-dependent transcription was defined for relative expression differences between 786-O and 786-OpVHL$_{30}$ if $0.6 \geq x \geq 1.75$. Deregulated proteins are marked in **bold**.

Table W8. List of Candidates Analyzed for mRNA Expression in the Two Major Subtypes of RCC (ccRCC *vs* pRCC).

No.	Gene Name	ccRCC/Normal	pRCC/Normal	Ratio ccRCC/pRCC	*P* value RNA Expression ccRCC *vs* Normal	Differential Expression Tissue ccRCC *vs* Normal, ccRCC *vs* pRCC	Differential Expression Tissue and Cell Lines
1	***AXL***	**2.44**	**1.59**	**1.53**	**.0036**	**1**	**1**
2	***BCAM***	**0.23**	**0.16**	**1.45**	**.0000**	**1**	**1**
3	***CDH2***	**4.88**	**5.88**	**0.83**	**.0052**	**1**	**1**
4	***CDH6***	**3.40**	**12.42**	**0.27**	**.0022**	**1**	**1**
5	***F3***	**0.10**	**0.16**	**0.58**	**.0000**	**1**	**1**
6	***HEG1***	**0.57**	**0.26**	**2.24**	**.1700**	**1**	**1**
7	***MME***	**0.77**	**0.08**	**9.81**	**.0700**	**1**	**1**
8	***SLC22A4***	**13.88**	**4.56**	**3.04**	**.0304**	**1**	**1**
9	***SLC2A1***	**2.21**	**0.26**	**8.55**	**.0191**	**1**	**1**
10	*BST2*	2.13	0.31	6.92	.0284	1	0
11	*CD82*	0.16	0.10	1.57	.0000	1	0
12	*CDCP1*	0.26	1.32	0.20	.0031	1	0
13	*CDH13*	2.47	0.12	20.61	.0312	1	0
14	*ENPEP*	3.97	0.45	8.93	.0022	1	0
15	*GPR126*	4.31	6.17	0.70	.0227	1	0
16	*HLA-B, MICA*	3.55	1.23	2.89	.0363	1	0
17	*HSPG2*	1.32	0.25	5.34	.2400	1	0
18	*ITGA1*	1.54	0.27	5.74	.0800	1	0
19	*ITGA5*	2.24	0.51	4.43	.0500	1	0
20	*MCAM*	4.15	0.78	5.35	.0139	1	0
21	*NCAM1*	0.27	0.13	2.08	.0043	1	0
22	*PROCR*	2.86	0.79	3.63	.0096	1	0
23	*SCARB1*	35.98	3.45	10.44	.0061	1	0
24	*SLC4A7*	0.29	0.24	1.21	.0002	1	0
25	*SLC6A6*	0.30	0.99	0.30	.0000	1	0
26	*THBS1*	0.55	0.17	3.34	.0022	1	0
27	*TNC*	0.10	0.28	0.34	.0000	1	0
28	*VCAM1*	3.90	4.91	0.79	.0034	1	0
29	*DPP4*	1.94	3.76	0.51	.0206	0	1
30	*ABCB1*	0.63	1.67	0.38	.0034	0	0
31	*ADAM10*	0.71	1.34	0.53	.0008	0	0
32	*ADCY9*	1.12	0.93	1.21	.4100	0	0
33	*ALCAM*	1.68	1.21	1.39	.0080	0	0
34	*ANPEP*	0.48	1.13	0.42	.0086	0	0
35	*ATP1B1*	0.33	0.51	0.65	.0000	0	0
36	*BSG*	0.86	0.99	0.86	.2200	0	0
37	*CA12*	0.61	0.41	1.51	.0013	0	0
38	*CD109*	2.49	2.09	1.19	.0235	0	0
39	*CD276*	2.31	2.39	0.97	.0289	0	0
40	*CD40*	2.84	1.04	2.73	.0108	0	0
41	*CD44*	1.07	1.02	1.05	.7400	0	0
42	*CD47*	1.44	1.64	0.88	.0700	0	0
43	*CD63*	1.38	1.43	0.96	.0297	0	0
44	*CD97*	1.35	1.32	1.02	.2600	0	0
45	*CLDND1*	1.15	0.68	1.69	.3600	0	0
46	*DSG2*	1.38	2.02	0.68	.3000	0	0
47	*ECE1*	0.95	0.55	1.73	.7200	0	0
48	*EGFR*	2.16	1.15	1.88	.0700	0	0
49	*EPHA2*	0.67	0.67	1.01	.0496	0	0
50	*GFRA1*	1.74	1.14	1.53	.4200	0	0
51	*GPC1*	1.41	1.93	0.73	.1100	0	0
52	*ICAM1*	1.36	0.69	1.97	.0266	0	0
53	*ITFG3*	0.78	1.20	0.65	.0010	0	0
54	*ITGA3*	0.79	2.53	0.31	.0346	0	0
55	*KIRREL*	1.18	0.72	1.65	.4200	0	0
56	*LTBR*	1.85	1.88	0.99	.0017	0	0
57	*M6PR*	0.84	0.90	0.94	.4100	0	0
58	*MPZL1*	1.85	2.81	0.66	.0078	0	0
59	*NCSTN*	0.97	0.98	0.99	.4800	0	0
60	*NPTN*	0.32	0.21	1.53	.0004	0	0
61	*NRP1*	2.05	0.80	2.56	.0079	0	0
62	*OSMR*	1.07	0.99	1.08	.6700	0	0
63	*PLXNB2*	0.65	0.72	0.90	.0003	0	0
64	*PTPRF*	0.78	0.79	0.99	.0600	0	0
65	*PTPRJ*	0.46	0.79	0.58	.0001	0	0
66	*PTPRK*	1.39	2.17	0.64	.1200	0	0
67	*SLC39A6*	0.68	0.64	1.07	.0306	0	0
68	*SLC3A2*	0.67	0.59	1.13	.0021	0	0
69	*SLC44A2*	0.60	0.80	0.75	.0051	0	0
70	*SLC7A1*	0.67	0.35	1.91	.0489	0	0
71	*TMEM2*	2.15	1.31	1.65	.0205	0	0
72	*TMEM30A*	0.78	0.60	1.30	.1000	0	0
73	*TPBG*	0.36	0.68	0.53	.0004	0	0

A *P* value is given for the significance of different mRNA expression in the RCC subtypes. Candidates with different expression in both tissues and cell lines are in **bold**. Differential expression is defined as $0.5 > x > 2$.

Table W9. List of Primers Used in This Study.

Primer Name	Sequence
Primers used for the generation of CD10 reporter constructs	
CD10 (−5134/−1005) f	5′-ATG CGG TAC CAG CCC ACA TTT TCA CTT TGC-3′
CD10 (−5134/−1005) r	5′-ATG CGC TAG CAC AGC AGA ATG GCA AAT TCC-3′
CD10 (−5134/−3744) f	5′-ATG CGG TAC CAG CCC ACA TTT TCA CTT TGC-3′
CD10 (−5134/−3744) r	5′-ATG CGC TAG CTG AGG GTC TGA CTG TGT TGC-3′
CD10 (−3763/−2391) f	5′-ATG CGG TAC CGG GAG ATG TGG GTA GTC CAA-3′
CD10 (−3763/−2391) r	5′-ATG CGC TAG CTG AGG GTC TGA CTG TGT TGC-3′
CD10 (−2557/−1005) f	5′-ATG CGG TAC CCT TTG AGG AGG AAT CGC TGT-3′
CD10 (−2557/−1005) r	5′-ATG CGC TAG CAC AGC AGA ATG GCA AAT TCC-3′
CD10 MUT f	5′-GCC AAC CGA CCT CCT ACA TCA TAA AAT GAC TAA GAA GGT CTC ACC-3′
CD10 MUT r	5′-GGT GAG ACC TTC TTA GTC ATT TTA TGA TGT AGG AGG TCG GTT GGC-3′
Primers used for the ChIP analysis	
KCNJ5_FW	5′-ACC TTA AGC TGT TAC TGG GTC TGG C-3′
KCNJ5_RW	5′-GCC AGA CCC AGT ATC AGC TTA AGG T-3′
HREI_FW	5′-TTT TGG CTG GCT TCT TTA CA-3′
HREI_RW	5′-GGG TAA AAT AAG GCT GAG ACC TG-3′
HREII_FW	5′-AAT TAG CTC GGT GTG GTG GT-3′
HREII_RW	5′-CTG GAG TGC AGT GGT GTG AT-3′
HREIII_FW	5′-TGG ATT CAG GGA GGA AAG G-3′
HREIII_RW	5′-AAC AAT ACA CGG GCT CTT CG-3′
HREIV_FW	5′-GTC CGC AGC TAA GGT CCA G-3′
HREIV_RW	5′-CTC TCC CTC CCC TCA CTC TT-3′

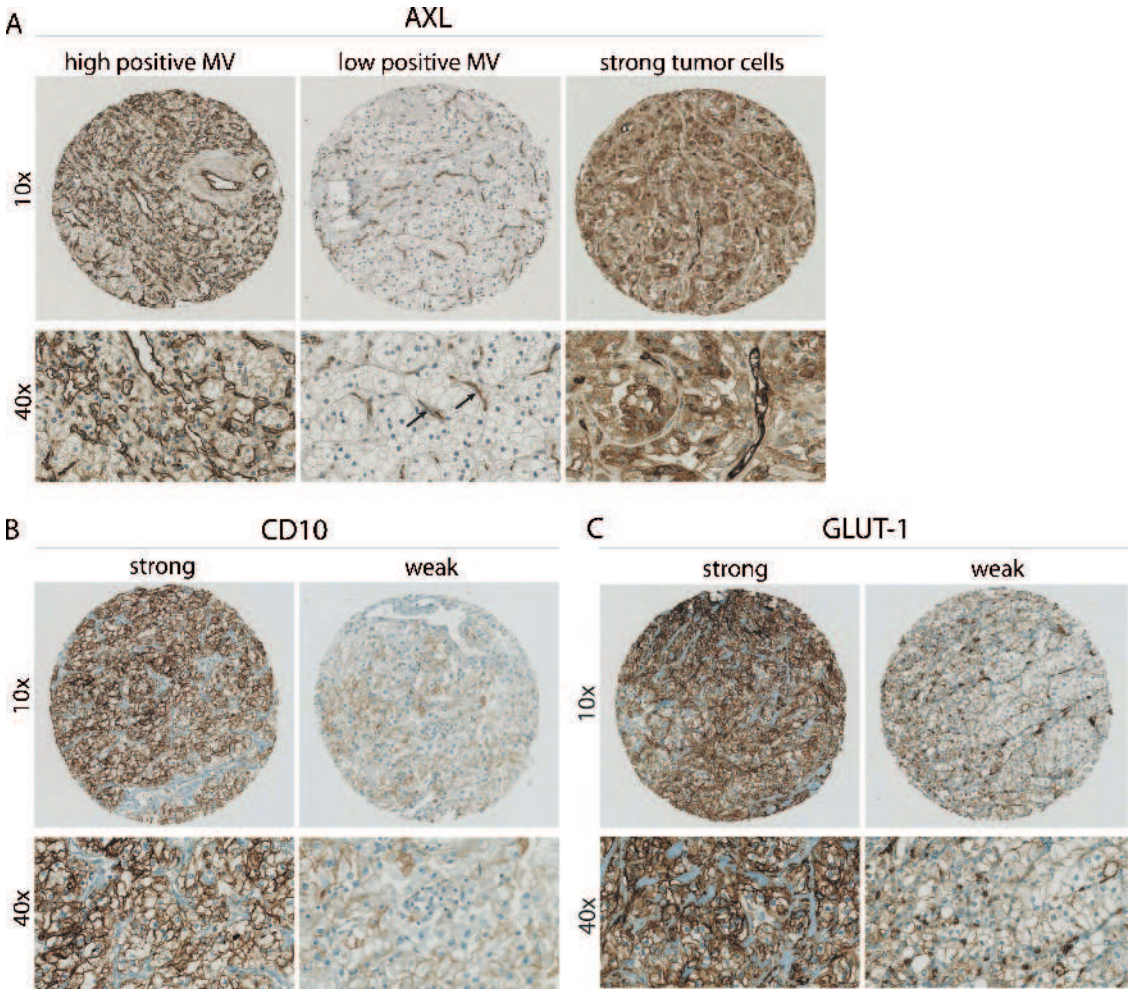

Figure W2. Representative pictures of ccRCC immunohistochemically analyzed with antibodies against AXL, CD10, and GLUT-1. The magnification of the pictures is indicated (10×, 40×). (A) AXL expression in ccRCC. From left to the right: ccRCC with many strong positive endothelial cells in microvessels (MVs) and weak cytoplasmatic staining of tumor cells. ccRCC with sparse strong positive endothelial cells and negatively stained tumor cells. Strong cytoplasmatic expression of AXL in tumor cells. Microvessels are indicated by arrows. (B) CD10 expression in ccRCC. Strong and weak membranous expression of CD10. (C) GLUT-1 expression in ccRCC. Strong and weak membranous expression of GLUT-1. Erythrocytes are strong positive and serve as internal control for the staining.